

# Integration of a DC/DC converter in the High Voltage System for Fuel Cell Cars

Design, Simulation and comparison of a 45kW isolated and a non-isolated DC/DC converter

Master's thesis in Electric Power Engineering

YEONGJU JIN, AKSHAY PRAKASH MAHAJAN



MASTER'S THESIS 2019

# **Integration of a DC/DC converter in the High Voltage System for a Fuel Cell Car**

Design, Simulation and comparison of a 45kW isolated and a non-isolated DC/DC converter

YEONGJU JIN, AKSHAY PRAKASH MAHAJAN



**CHALMERS**  
UNIVERSITY OF TECHNOLOGY

Department of Electrical Engineering  
*Division of Electric Power Engineering*  
CHALMERS UNIVERSITY OF TECHNOLOGY  
Gothenburg, Sweden 2019

YEONGJU JIN, AKSHAY PRAKASH MAHAJAN

© YEONGJU JIN, AKSHAY PRAKASH MAHAJAN 2019.

Supervisor: Björn Isaksson, CEVT

Examiner: Torbjörn Thiringer, Electric Power Engineering Department

Master's Thesis 2019

Department of Electrical Engineering

Division of Electric Power Engineering

Chalmers University of Technology

SE-412 96 Gothenburg

Telephone +46 31 772 1000

Typeset in L<sup>A</sup>T<sub>E</sub>X

Printed by Chalmers Reproservice

Gothenburg, Sweden 2019

## **Integration of a DC/DC converter in the High Voltage System for a fuel cell car**

Design, Simulation and comparison of a 45kW isolated and a non-isolated DC/DC converter

AKSHAY MAHAJAN, YEONGJU JIN

Department of Electrical Engineering

Division of Electric Power Engineering

Chalmers University of Technology

### **Abstract**

Electrification in the automotive industry has created huge interest in the fuel cell technology. The DC-DC converter acts as a key component in a fuel cell vehicle. The safety and packaging concerns make integration of a DC-DC into the car crucial. In this thesis, different topologies of the DC-DC are evaluated and simulated for its efficiency, cost and volume analysis. The DC-DC is designed in MATLAB and SIMULINK to step up the voltage from a minimum input of 90 V to a maximum output of 378 V between the fuel cell and the inverter.

This thesis also discusses in detail, an inductor design for the non isolated topology and a transformer for the isolated topology. An efficient way to supply power to the air compressor of the fuel cell is also discussed. It is seen that the non isolated converter has a higher efficiency of 99 % than that of the isolated converter which is 95.3 %. However, the cost and the volume with the selected components for the isolated converter is higher than that for the non isolated converter. Also, safety concerns and complications on account of the high short circuit protection needed for the fuel cell has made us adopt the isolated topology for the fuel cell car.

Keywords: DC-DC converter, Fuel cell car application, Magnetic circuit design, three-phase boost converter, isolated full-bridge converter



## **Acknowledgements**

We would like to thank our supervisors at CEVT, Björn Isaksson and Bengt Axelsson for providing us the opportunity to conduct the interesting thesis project at CEVT. Their support and knowledge have been valuable resources throughout the our whole project.

Further, we would like to thank our examiner Dr. Torbjörn Thiringer at the division of Electric Power Engineering, Chalmers University of Technology. His patience and guidance with helpful input throughout the thesis has been of great importance.

A special thanks to Robert Karlsson at the division of Electric Power Engineering, Chalmers University of Technology for his valuable inputs.

YEONGJU JIN, AKSHAY PRAKASH MAHAJAN, Gothenburg, 06,2019



# Contents

<b>1</b>	<b>Introduction</b>	<b>1</b>
1.1	Problem background . . . . .	1
1.2	Previous work . . . . .	1
1.3	Purpose . . . . .	2
1.4	Scope . . . . .	2
1.5	Sustainability aspect . . . . .	2
<b>2</b>	<b>Theoretical Background</b>	<b>5</b>
2.1	Review of fuel cell and fuel cell car . . . . .	5
2.1.1	Powertrain Schematic of a fuel cell car and its Working principle . . . . .	5
2.1.2	Working principle of fuel cell and its characteristics . . . . .	7
2.1.3	Electrical safety requirements in a fuel cell car . . . . .	8
2.2	Circuit components . . . . .	9
2.2.1	Power MOSFET . . . . .	9
2.2.2	Diode . . . . .	10
2.2.3	Input filter . . . . .	11
2.2.4	Output filter . . . . .	11
2.2.5	Heat Sink Design . . . . .	12
2.3	DC/DC converter topology review . . . . .	12
2.3.1	Isolated Full bridge-fullwave bridge . . . . .	13
2.3.2	Unisolated three-level boost converter . . . . .	13
2.3.3	Unisolated three-phase boost converter . . . . .	14
2.3.4	Unisolated buck-boost converter . . . . .	15
2.4	Magnetic component design . . . . .	16
2.4.1	Transformer design for isolated converters . . . . .	16
2.4.2	Inductor design for nonisolated converters . . . . .	19
2.4.3	Core selection . . . . .	21
2.4.4	Wire selection . . . . .	21
2.5	Pulse width modulation (PWM) . . . . .	22
2.6	Varying voltage drive system . . . . .	23
<b>3</b>	<b>Case set-up</b>	<b>25</b>
3.1	DC/DC converter design and simulation cases . . . . .	25
3.2	Design A . . . . .	27
3.2.1	DC/DC Converter topology selection process for design and simulation . . . . .	27

3.2.2	DC/DC converter components selection for simulation and volume packaging . . . . .	29
3.2.2.1	Component rating selection . . . . .	29
3.2.2.2	Transformer selection . . . . .	29
3.2.2.3	Inductor selection . . . . .	30
3.2.3	Base verification . . . . .	30
3.2.3.1	Base boost converter . . . . .	30
3.2.3.2	Full bridge converter with two legs . . . . .	32
3.3	Comparison with varying voltage system . . . . .	32
3.4	INN balance car . . . . .	33
3.4.1	Simple buckboost converter . . . . .	33
<b>4</b>	<b>Analysis</b>	<b>35</b>
4.1	Design A . . . . .	35
4.1.1	Isolated Full bridge - full wave unidirectional DC/DC converter . . . . .	35
4.1.1.1	Loss calculation . . . . .	35
4.1.1.2	Control strategy . . . . .	41
4.1.1.3	Transformer and wire setup for B core in Table 2.1 . . . . .	41
4.1.1.4	Simulation . . . . .	45
4.1.1.5	Cost analysis . . . . .	46
4.1.1.6	Dual active bridge cost analysis . . . . .	49
4.1.1.7	Volume Analysis . . . . .	49
4.1.2	Non-isolated three-level boost converter . . . . .	52
4.1.2.1	Control Strategy . . . . .	52
4.1.2.2	Simulation . . . . .	53
4.1.3	Non-isolated three-phase boost converter . . . . .	54
4.1.3.1	Loss calculation . . . . .	54
4.1.3.2	Control strategy . . . . .	57
4.1.3.3	Inductor and wire setup . . . . .	57
4.1.3.4	Simulation . . . . .	60
4.1.3.5	Cost analysis . . . . .	62
4.1.3.6	Volume analysis . . . . .	64
4.2	Design B . . . . .	67
4.2.1	Non-isolated buck-boost converter . . . . .	67
4.2.1.1	Simulation . . . . .	67
<b>5</b>	<b>Conclusion</b>	<b>69</b>
5.1	Efficiency . . . . .	69
5.2	Cost Analysis . . . . .	70
5.3	Volume Analysis . . . . .	70
<b>6</b>	<b>Future work</b>	<b>73</b>
	<b>Bibliography</b>	<b>75</b>

# 1

## Introduction

### 1.1 Problem background

The interest and concern in environmental issues have increased. United Nations Economic Commission for Europe (UNECE) decided to switch from the New European Driving Cycle (NEDC) to Worldwide Harmonised Light Vehicle Test Procedure (WLTP), effective from September 2017. The WLTP laboratory test has been designed to measure fuel consumption and CO<sub>2</sub> emissions from passenger cars, as well as their pollutant emissions. The purpose of the standardized test is to regulate fuel consumption and CO<sub>2</sub> emissions from cars. [1]

In order to meet this regulation and protect the environment, hybrid vehicles, battery electric vehicles and fuel cell vehicles could be a part of the solution. Fuel cell vehicles are the main topic of this thesis. This is because the adoption of the fuel cell in vehicles has helped to reach increased driving range capability. It is known that the main component in a fuel cell drive system is a DC/DC converter which acts as a power flow unit between the fuel cell stack and an inverter. In this thesis, further research on a DC/DC converter in fuel cell vehicles will be conducted.

### 1.2 Previous work

There has been a lot of research on the DC/DC converters for fuel cell applications in terms of design and verification [2], [3],[4] and even fuel cell cars without DCDC converters [5]. In [2] and In [3], design and simulation of a 1.2kW isolated half-bridge push-pull converter power circuit for the fuel cell are introduced. On the other hand, in [4], design and prototype test of 100kW non-isolated boost converter for a fuel cell are carried out.

However, there was not much information about the integration of the DC/DC converter into fuel cell cars and comparing the efficiency, cost and volume analysis of the DC/DC converter with both an isolated and unisolated converter topology in the fuel cell car.

### 1.3 Purpose

This purpose of this project is to make an integration of a DC/DC converter in the High Voltage Energy Storage System of a fuel cell car and compare cost, efficiency and volume for different topologies of a DC/DC converter.

### 1.4 Scope

The main work is to design and compare DC/DC converters with several topologies and parameters of the powertrain. The dc/dc topology will be analyzed based on cost, efficiency, safety requirements and volume. Literature study on converters and fuel cell gives a clear idea about how the energy flow in the car will look like in different scenarios.

Different topologies will be designed for deciding whether to use an isolated or an unisolated converter in terms of efficiency. The designed DC/DC converter will be simulated with SIMULINK to verify the calculation. Then the components will be selected to have low cost, low volume, and high efficiency. If time permits the designed converter circuit will be drawn on PCBs in accordance with ISO standard. The volume analysis will be done to compare isolated converters and non-isolated converters.

The feasibility of having the DC/DC converter in the high voltage system in fuel cell vehicles will be discussed. The concept of fuel cell vehicles with the DC/DC converter and without the DC/DC converter, so-called varying voltage system will be compared for efficiency and cost.

If time allows, thermal simulation of the designed DC/DC converter in COMSOL Multiphysics will be conducted to propose the most appropriate cooling system in cost, efficiency and volume wise.

The whole analysis will be done based on the information we get from the market survey and the supplier.

Due to the limited time period, manufacture and test of PCBs will not be covered in this thesis as well as controllers and gate drives of MOSFETs. Still, when it comes to controllers, control strategy will be suggested. Degradation due to heat will not be considered in this thesis as well.

### 1.5 Sustainability aspect

This section discusses the sustainability aspects involved for the design and in which way this thesis has contributed to the environment. Fuel cell vehicles have many benefits when it comes to the environmental aspects. Although they cause no pollution [23], some aspects of the design must be taken into account for their contribution to the environment. When it comes to manufacturing a fuel cell high efficiency, low cost and low volume can

be criterias but also making it environmentally beneficial is vital. In this thesis, the components used have the certification of RoHS(Restriction of Hazardous substances). RoHS limits the use of 6 toxic substances in the electrical industry [24].

For the transformer and the inductor design, maximum current density values have been chosen for the windings so that a low amount of copper is used. In this way the electronic wastes are reduced. When considering the PCB design, a maximum proportion for the soldering is of tin which contributes to the environment as compared to the traditional material used in soldering i.e lead [24].

The materials used for production of other vital components in a fuel cell vehicle should also be taken into consideration for ethical aspects. Production of a Lithium ion battery, especially in areas where Lithium is abundant has caused a major concern for exploitation of the residents near these areas. They can become a source of cheap labour and so immense work is required to reduce the problems associated with Lithium production to make it ethical[25].



# 2

## Theoretical Background

### 2.1 Review of fuel cell and fuel cell car

In this section, characteristics of fuel cells and fuel cell cars are explained.

#### 2.1.1 Powertrain Schematic of a fuel cell car and its Working principle

The proposed fuel cell car powertrain schematic and description of the main components in the powertrain are discussed in this chapter.

A proposed matrix has been put forward and is currently in discussion for different combinations of a fuel cell stack, battery, electric motors and a DC/DC converter. The electric motor capacity with a 150 kW, fuel cell stack with a capacity of 45 kW, the battery with 90 cells in series and a capacity of 9.7 kWhr. A DC/DC converter between the fuel cell stack and inverter. The schematic can be seen in Figure 2.1. The DC/DC boost converter is very close to the fuel cell stack. The DC link, in our case, is varying between 324 V-378 V.

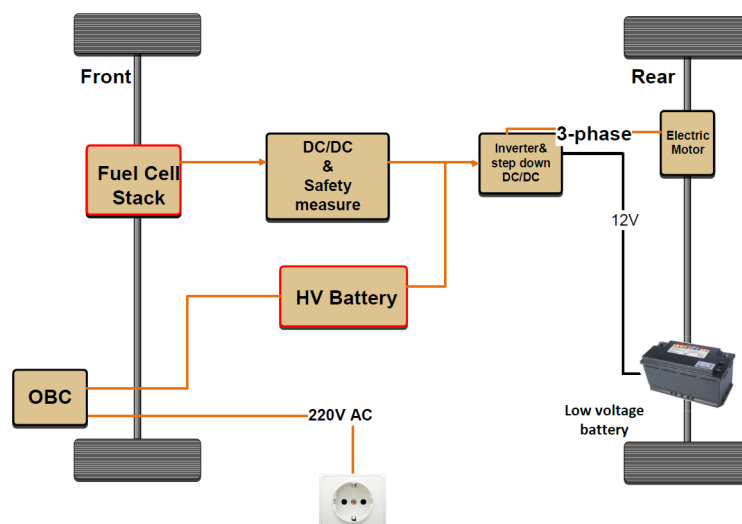


**Figure 2.1:** Powertrain schematic of a fuel cell car

Also, this car will have an onboard charger (OBC), which can be seen in the bottom middle of Figure 2.1.

## 2. Theoretical Background

---

As can be seen in Figure 2.1, a fuel cell prototype car will have a system that fuel cell stack is the main power source and with a high voltage battery as an additional power source, a DC/DC converter for fuel cell stack, an inverter and an electric motor.

When the car is powered on, a fuel tank and an air compressor start running with power from the high voltage battery power and supply fuel and oxygen to fuel cell stack. Until the fuel cell stack has sufficient power to support the load, the car is only able to operate with battery power.

When a driver speeds up the car, the fuel cell will supply power to the load. However, when higher power is needed, the battery will assist the fuel cell stack to supply power to the load since the fuel cells have lower power density. Having a high voltage battery in the system will enable regenerative braking during speed reduction of the car.

Since a fuel cell stack works as an electric generator rather than an electric battery, a turn-off of the fuel tank and the air compressor will lead to a shutdown of the car. In other words, when the supply of fuel and oxygen is stopped, the fuel cell stack cannot supply electricity to the load.

Another proposal (B) is to start the compressor with power from a bidirectional DC-DC eventually coming from the HV battery as seen in the Figure 2.2.

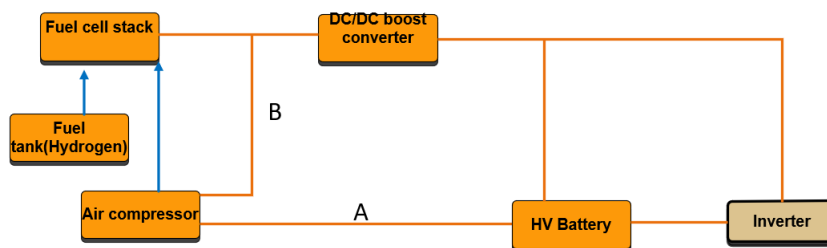


**Figure 2.2:** Power flow schematic for the compressor

**Case I.** In Figure 2.2 Path A suggests continuous supply to the compressor from the HV battery. This can lead to continuous use of the battery and hence charging will be required frequently. A unidirectional DC-DC is needed in this case.

**Case II.** In path B, power is supplied via the DC-DC so there will be loss of efficiency. Also more Short circuit protection is needed because of the bidirectional power flow. However the pros are that the battery can be used only during the starting of the car and the remaining time the fuel cell can provide power. Thus there is less energy loss. A bidirectional DC-DC is needed in this case.

**Case III.** In case of both path A and B being used, HV battery can start up the compressor via path A and the remaining time the fuel cell can supply the required power. Thus there

is no need for a bidirectional DC-DC.

### 2.1.2 Working principle of fuel cell and its characteristics

Fuel cells are electrochemical energy conversion devices. There are many types of fuel cells depending on fuel, but in this thesis, Proton-exchange membrane fuel cells or polymer electrolyte membrane (PEMFC) will be used.

When both fuel ( $H_2$ ) on the anode and air ( $O_2$ ) on the cathode side of the cell arrive at the electrolyte barrier (membrane) which separates two electrodes, electrons from  $H_2$  flows into the external electric circuit and arrive at the cathode. Protons from  $H_2$  pass through the electrolyte barrier and arrive at the cathode side, reacting with  $O_2$  and electrons, and resulting in water as its byproduct.

Fuel cells are well known for low voltage to be high current power sources. Its cell voltage and current density characteristics are shown in Figure 2.3.

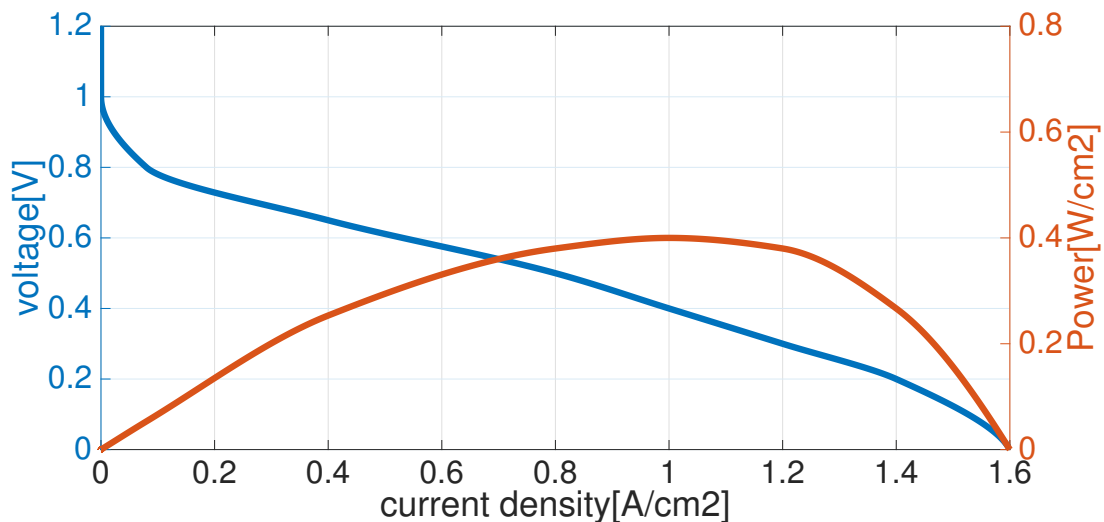


**Figure 2.3:** Fuel cell V-I characteristics [6]

In addition, fuel cells are known as having lower power density while having a higher energy density, meaning that a fuel cell cannot support higher power than a battery can but it can last longer than a battery.

### 2.1.3 Electrical safety requirements in a fuel cell car

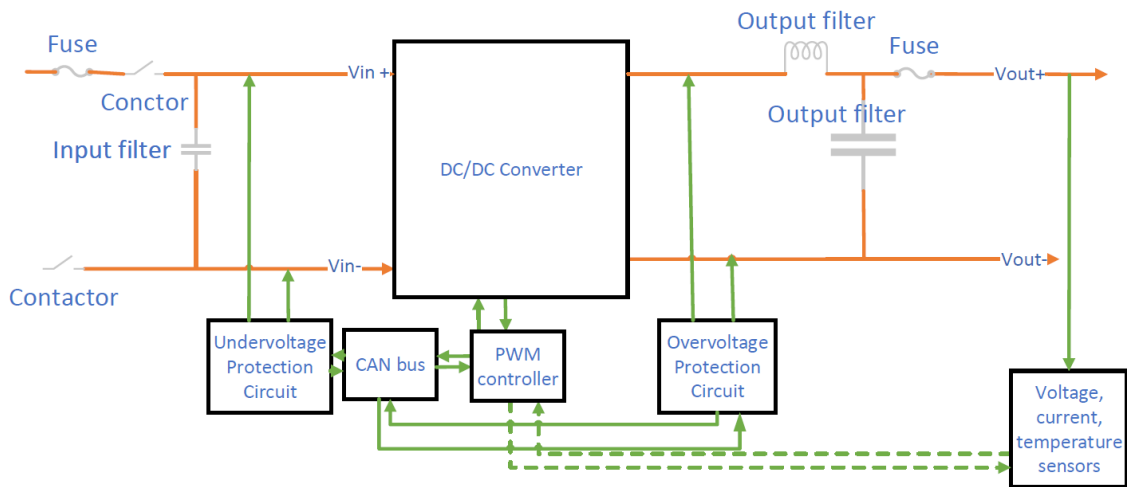


**Figure 2.4:** Safety Requirement of DC/DC converter in the FC car

In Figure 2.4, electrical safety requirements for a fuel cell car are depicted.

First of all, two high voltage fuses are placed on both the primary and on the secondary side of the DC/DC converter to protect both sides of the converter due to overcurrent and short circuit current. Also, under voltage and overvoltage protection circuits are included to protect the converter from malfunction or damage. Input and output filters are included to reduce noises.

The DC/DC converter can be either one of two: isolated or nonisolated. Isolation between the primary and the secondary side of the converter provides protection of the fuel cell stack from faults within the battery and the inverter side, such as short circuit of high voltage system poles or high voltage system insulation issues. In this case, two contactors on the fuel cell sides are redundant. On the other hand, non-isolation should come with the two contactors. Otherwise there is no way to disconnect the fuel cell stack from the battery or inverter side which might have higher voltage than the fuel cell.

The advantage of having an isolator in this application, where the maximum output voltage of the DC/DC converter is more than four times the minimum input voltage, is that the fuel cell stack are protected from the high voltage on the car and the battery side by the DC/DC converter. Also, the isolator acts as a boosting up element for the input voltage, reducing the maximum duty cycle.

The disadvantage of having an isolator is that it will end up with higher volume, higher cost and lesser efficiency than unisolated converters.

The efficiency, volume and cost of unisolated converters will be compared with isolated converters for this application. The advantage of having unisolated converters is that it will cost less, have lesser volume and higher efficiency than isolated converters.

However, unisolated topology will face safety problems. Thus, in case of not having isolation, a contactor at each pole between the DC/DC converter and the inverter side is to be placed for isolation purpose, implying that there is no galvanic isolation between input and output side when the DC/DC converter is in operation. This means contactors should be quick enough to prevent DC/DC converters and also fuel cell stack from damaging. If the contactors have control issue or welded, fuel cell stack is exposed to high voltage on vehicle or battery side. In addition, in this application, the inductors for stepping up the voltage will be huge, increasing volumes.

## 2.2 Circuit components

In this section, power dissipation and value selection of the circuit components will be covered.

### 2.2.1 Power MOSFET

A power MOSFET is a semiconductor device which has high switching speed mostly used for voltages below 200V. It has two intrinsic capacitances which must be charged and discharged during the switching operation. The charging and the discharging time decides the commutation time of the MOSFET. The N-channel MOSFET is the most commonly used MOSFET in the industry [7].

Power MOSFET losses can be divided into four categories, Switching, conduction, dead time and gate charging time losses according to [8].

$$P_{MOSFET} = P_{sw} + P_{cond} + P_{dt} + P_{gate} \quad (2.1)$$

The total MOSFET losses are obtained by multiplying the number of MOSFETs in converters.

The switching loss is characterized by considering the ON and OFF intervals through the following expression,

$$P_{sw} = V_{in} I_{in} f_{sw} \left( \frac{t_r + t_f}{2} \right) \quad (2.2)$$

For the case with MOSFETs only on the input side,  $V_{in}$  is the input voltage,  $I_{in}$  is the input current,  $f_{sw}$  is the switching frequency.  $t_r$  and  $t_f$  is the rise time and fall time respectively.

When there are two converters connected in parallel, for instance as in a full bridge converter,  $I_{in}$  is divided by two. If there are three phases in a boost converter,  $I_{in}$  is divided by three.

## 2. Theoretical Background

---

The conduction losses are calculated using

$$P_{cond} = (I_{in}^2)R_{on}D \quad (2.3)$$

where  $R_{on}$  is the on state resistance of the MOSFET,  $I_{in}$  is the input current through the drain to source and  $D$  is the duty cycle.

Dead time is introduced to avoid the high current spikes between  $V_{in}$  and GND by controlling the turn ON time of the MOSFETs of the same leg. The dead time losses are given by

$$P_{dt} = V_{sd}I_{in}(t_{dtr} + t_{dtf})f_{sw} \quad (2.4)$$

where  $V_{sd}$  is the body diode forward voltage,  $t_{dtr}$  and  $t_{dtf}$  are rise time and fall time during the dead time interval.

MOSFET gate charging loss is given by

$$P_{gate} = Q_{g_{tot}}V_{gs}f_{sw} \quad (2.5)$$

where  $Q_{g_{tot}}$  is the total gate charge.

MOSFET gate drive losses are neglected since gate drives and PWM controllers are not included in this thesis and losses are small enough to neglect.

### 2.2.2 Diode

Diode losses in power converters are too high to neglect. The losses also depend on where the diodes are located. In general, the diode losses consist of three: conduction loss, off-time loss and switching loss, and it is calculated by

$$P_{diode} = P_{cond.diode} + P_{off.diode} + P_{sw.diode} \quad (2.6)$$

The total diode power loss is calculated by multiplying the number of diodes in converters into  $P_{diode}$ .

The conduction loss  $P_{cond.diode}$  occurs when diodes are in conduction mode, i.e., when current is flowing through the diode. The off time loss  $P_{off.diode}$  occurs due to its reverse recovery current and reverse blocking voltage. The switching loss  $P_{sw.diode}$  occurs due to switching of diodes during off time.

The conduction loss is calculated by

$$P_{cond.diode} = V_f \cdot I_f \quad (2.7)$$

where  $V_f$  means diode forward voltage drop,  $I_f$  is diode current during conduction mode.

In full-bridge converters, diodes are located on the output side. Thus, the diode current for full-bridge converters  $I_{f.FB}$  is calculated by

$$I_{f.FB} = \frac{P_{in} - P_{MOSFET}}{V_{out}} \quad (2.8)$$

In boost converters, diodes are located between input and output side and are in conduction mode during the switch-off period. Thus, the diode current for boost converters  $I_{f.boost}$  is calculated by

$$I_{f.boost} = I_{in}(1 - D) \quad (2.9)$$

where  $D$  is duty cycle.

The off time loss is calculated by

$$P_{off.diode} = V_{reverse}I_{reverse}(1 - D) \quad (2.10)$$

where  $V_{reverse}$  is the reverse blocking voltage and  $I_{reverse}$  is the reverse recovery current. Both characteristics are specified in the datasheets of diodes.

The switching loss is calculated by

$$P_{sw.diode} = E_{rr}f_{sw} \quad (2.11)$$

where  $E_{rr}$  is reverse recovery charging and calculated by

$$E_{rr} = \frac{I_{reverse.peak}t_{rr}}{2} \quad (2.12)$$

where  $I_{reverse.peak}$  is peak reverse recovery current and  $t_{rr}$  is the reverse recovery time, both of which are specified in datasheets.

### 2.2.3 Input filter

The input capacitor is designed to reduce the ripples in DC input current. The filter equation can be given by using

$$C_{in} = \frac{\Delta I_L}{8f_{sw}\Delta V_{in}} \quad (2.13)$$

where  $\Delta V_{in}$  is designed to be 10% of  $V_{in}$ .  $V_{in}$  is the input voltage and  $f_{sw}$  is the switching frequency of the MOSFET's.

### 2.2.4 Output filter

The output capacitor is used for reducing the ripples in the DC output voltage and current. A capacitor on the HV side can be designed with an output ripple requirement of  $\Delta V_{out}$  by using

$$C_{out} = \frac{I_{out}t_{ON}}{\Delta V_{out}} \quad (2.14)$$

## 2. Theoretical Background

---

where  $\Delta V_{out}$  is designed to be 10% of  $V_o$ .  $V_o$  is the output voltage and  $t_{ON}$  is the ON time of the MOSFETs.

The output inductance is used to reduce current ripples on the output side of the isolated converter.

$$L_{out} = \frac{1}{(2\pi \cdot 0.1 f_{sw})^2 C_{out}} \quad (2.15)$$

where 0.1 means cutoff frequency is set to be 10% of switching frequency which is an approximate rule of thumb for practical applications.

### 2.2.5 Heat Sink Design

Heat sink is a vital element in an electronic circuit design as it gives an efficient path for the heat transfer to the ambient air and thus protecting the electronic devices.

The heat sink junction temperature is given by

$$T_j = \Sigma R_{th} P_d + T_{amb} \quad (2.16)$$

where  $\Sigma R_{th}$  is the summation of the thermal impedences of junction to case, case to sink and sink to ambient in  $^{\circ}C/W$ ,  $P_d$  is the power dissipation per MOSFET and  $T_{amb}$  is the ambient temperature in  $^{\circ}C$  [21].

For forced air cooling, factor  $F$  is introduced in the thermal impedance of sink to ambient [22].  $\Sigma R_{th}$  is given by

$$\Sigma R_{th} = R_{jc} + R_{cs} + \frac{R_{sa}}{F} \quad (2.17)$$

$F$  is given by the equation

$$F = \frac{4.3}{\sqrt{D}} \quad (2.18)$$

$D$  is the airflow in  $m^3/hr$ .

## 2.3 DC/DC converter topology review

The DC/DC converter topologies in consideration will be reviewed in this section. For the cost, volume and efficiency comparison, both non-isolated and isolated converters will be reviewed.

### 2.3.1 Isolated Full bridge-fullwave bridge

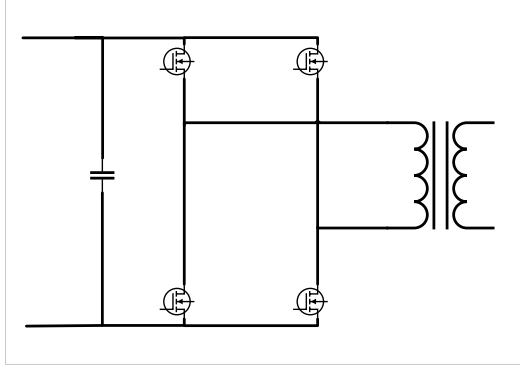


**Figure 2.5:** Primary side - Full bridge

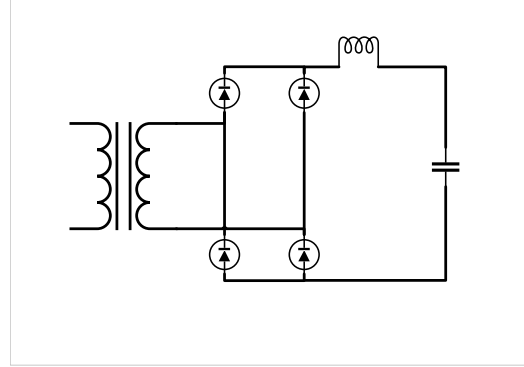


**Figure 2.6:** Secondary side - Fullwave bridge

The output voltage  $V_{out}$  and output current  $I_{out}$  on the secondary side are calculated by

$$V_{out} = 2D \frac{N_2}{N_1} V_{in} \quad (2.19)$$

and

$$I_{out} = \frac{P_{in} - P_{loss}}{V_{out}} \quad (2.20)$$

respectively, where  $P_{loss}$  is calculated by

$$P_{loss} = P_{cu} + P_{fe} + P_{MOSFET} + P_{diode} \quad (2.21)$$

The copper loss  $P_{cu}$  is calculated by (2.45), the core loss  $P_{fe}$  is calculated by (2.44), the MOSFET loss  $P_{MOSFET}$  is calculated by (2.1), and the diode loss  $P_{diode}$  is calculated by (2.6).

### 2.3.2 Unisolated three-level boost converter

In an unisolated boost converter, the energy storage element is the inductor on the input side. The three-level boost converter is shown in Figure 2.7.

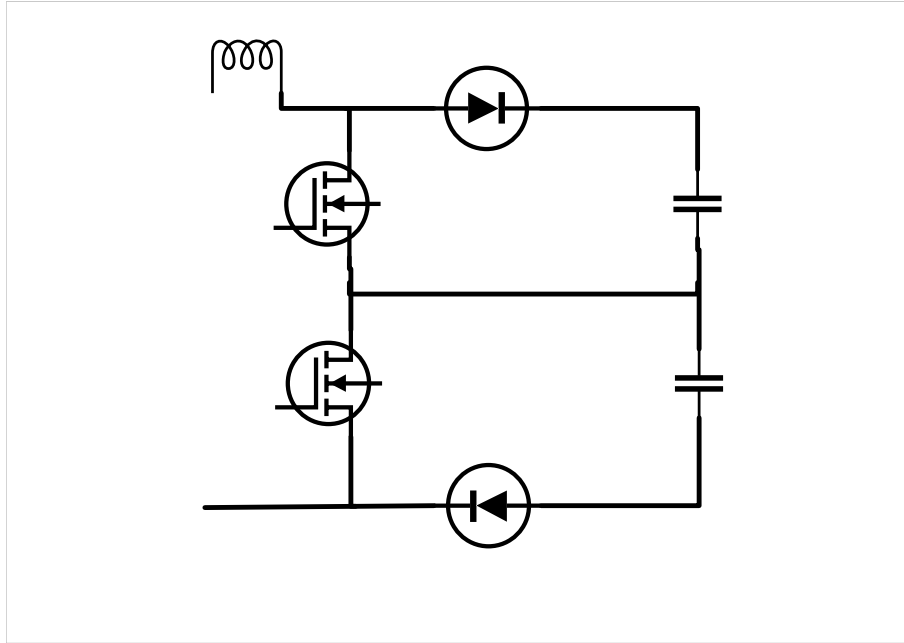


**Figure 2.7:** Three level boost converter model

The input and output voltage ratio is given by

$$\frac{V_{out}}{V_{in}} = \frac{1}{1-D} \quad (2.22)$$

where  $D$  is the duty cycle of both switches.

The maximum duty cycle  $D_{max}$  and the minimum duty cycle  $D_{min}$  are calculated by

$$D_{max} = \frac{V_{outmax} - V_{inmin}}{V_{outmax}} \quad D_{min} = \frac{V_{outmin} - V_{inmax}}{V_{outmin}} \quad (2.23)$$

The three-level boost converter in Figure 2.7 is controlled in such a way that two switches have a delay of 180 degrees each other. The inductor and the capacitors are calculated with (2.24) and (2.14).

$$L = \frac{V_{in}(V_{out} - V_{in})}{\Delta I_L f_{sw} V_{out}} \quad (2.24)$$

where  $\Delta I_L$  is the estimated inductor ripple current, i.e., 30% of input current per phase.

The Power loss is calculated by

$$P_{loss} = P_{MOSFET} + P_{diode} + P_{ind} \quad (2.25)$$

### 2.3.3 Unisolated three-phase boost converter

The inductor and the capacitors are calculated with (2.24) and (2.14). Power loss is calculated also by (2.25).

For volume analysis and switching frequency selection, it is important to know the total volumes of cores and wires.

$$V_{total} = (V_{core} + V_{wire})N_{ph} \quad (2.26)$$

where  $N_{ph}$  means the number of phases.  $V_{core}$  means the core volume and  $V_{wire}$  means the required wire volume and is calculated by (2.36).

### 2.3.4 Unisolated buck-boost converter

A buck-boost converter can be used for two major reasons, i.e., when the output voltage is both greater and less than input voltage in different cases respectively. The design in Simulink can be seen in Figure 2.8 below.

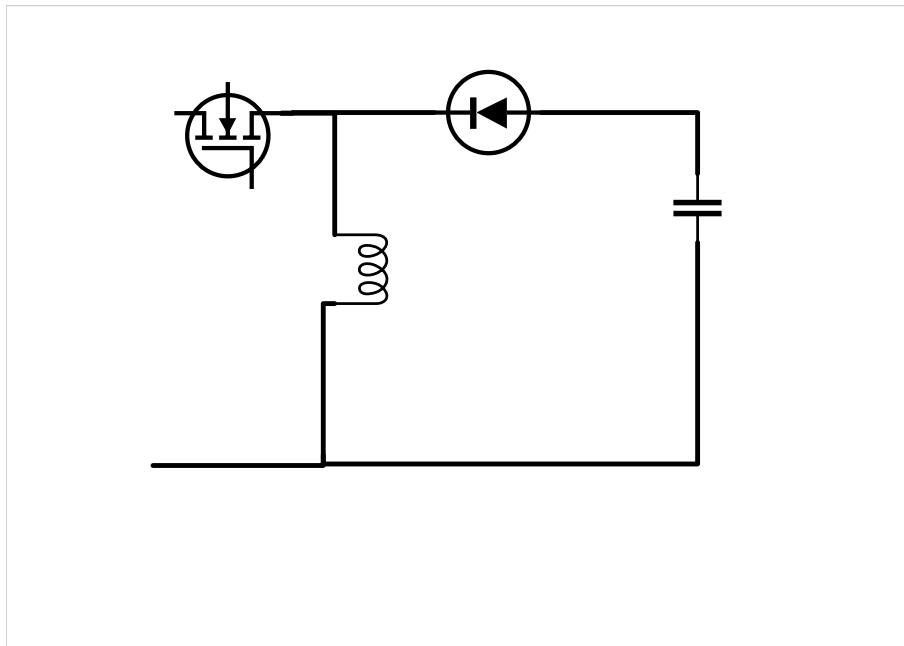


**Figure 2.8:** Buck Boost model

During on-time of the switch, the inductor is energized and the diode is reverse biased. Meanwhile, the output capacitor supplies energy to the load during the time when the inductor is building up the energy.

The inductor and the capacitor in a buck-boost converter is also calculated by (2.24) and (2.14), respectively.

The output voltage is given by

$$\frac{V_{out}}{V_{in}} = \frac{-D}{1-D} \quad (2.27)$$

where  $D$  is the duty cycle.

Power loss is calculated also by (2.25).

## 2.4 Magnetic component design

In this section, designing transformers for isolated topology and inductors for nonisolated topology are presented. Also, component candidates and selection criteria are listed as well.

### 2.4.1 Transformer design for isolated converters

A transformer for isolation of the primary and the secondary sides is designed for low volume and high efficiency. The Matlab code for transformer design is available in Appendix.

In order to calculate turns ratio, the first turns per volt is calculated by

$$TPV = \frac{1}{4BA_{core}f_{sw}} \quad (2.28)$$

The number 4 means that the waveform is a square wave,  $B$  means flux density. The core cross-section area  $A_{core}$  is in [ $m^2$ ] and switching frequency  $f_{sw}$  is in [Hz].

Thus the number of turns is calculated by

$$N_k = TPV \cdot V_k \quad (2.29)$$

where  $k$  indicates either the primary or the secondary side, being the primary when  $k=1$ , and the secondary when  $k=2$ .  $V$  is the voltage.  $N_k$  is rounded to nearest tenth to make into an integer.

When it comes to wires that realize the number of turns, it is important to use a wire that withstand the current with low resistance. Thus a wire with small radius is made into a bundle to meet both conditions.

The area of a bundle of wires  $A_{bundle.k}$  is calculated with

$$A_{bundle.k} = \frac{I_k}{J_{wire}} \quad k = 1, 2 \quad (2.30)$$

where  $I_k$  is the current that has to flow through the bundle of wires, determined by the power source and  $J_{wire}$  is current density of a selected wire.

To calculate how many wires are needed in one bundle,  $N_{wire.per.bundle}$  is calculated using

$$N_{wire.per.bundle.k} = \frac{A_{bundle.k}}{A_{wire}} \quad k = 1, 2 \quad (2.31)$$

where  $N_{wire.per.bundle}$  indicates the number of wires per bundle and  $\rho_{v.wire}$  indicates volume density of a wire.

The wire length is calculated with

$$l_{wire.k} = MLT_k N_k \quad k = 1, 2 \quad (2.32)$$

where  $MLT$  is mean length per turn determined by the selected core, and  $N$  is the number of turns.

$MLT$  is specified in the core datasheet, but still depends on the number of layers, core shapes, and whether a bobbin is used. The calculation of  $MLT$  depending on those factors are calculated by [10]

$$MLT_{1layer.k} = 2(l_{bobbin} + w_{bobbin} + \pi r_{bundle.k}) \quad k = 1, 2 \quad (2.33)$$

where  $l_{bobbin}$  and  $w_{bobbin}$  are bobbin size and  $r_{bundle}$  is radius of one bundle of wires. This means that (2.33) is mean length per turn when having one layer.

If there are more than one layer of winding around bobbin, the  $MLT$  of the second layer is calculated by [10]

$$MLT_{2layer.k} = 2(l_{bobbin} + w_{bobbin} + 3\pi r_{bundle.k}) \quad k = 1, 2 \quad (2.34)$$

The winding area  $A_{winding}$  which is determined by the number of turns per each side is calculated by

$$A_{winding.k} = (2r_{bundle.k})^2 N_{layer.k} N_k \quad k = 1, 2 \quad (2.35)$$

where  $N_{layer}$  is the number of winding layers and depends on height of a bobbin  $h_{bobbin}$  when a bobbin is used.  $r_{bundle}$  is radius of one bundle of wires.

The wire volume  $V_{wire}$  and mass  $M_{wire}$  are calculated with

$$V_{wire.k} = l_{wire.k} N_{wire.per.bundle.k} A_{wire} \quad k = 1, 2 \quad (2.36)$$

and

$$M_{wire.k} = V_{wire.k} \rho_{v.wire} \quad k = 1, 2 \quad (2.37)$$

respectively.

In addition, the primary and the secondary inductances without airgap are calculated by using

$$L_k = A_L N_k^2 \quad k = 1, 2 \quad (2.38)$$

where  $A_L$  is inductance factor and specified in the core datasheet. However, sometimes it is not specified and thus can be calculated by

$$A_L = \frac{\mu_0 \mu_{core} A_{core}}{l_m} \quad (2.39)$$

## 2. Theoretical Background

---

If the air gap exists in the transformer, the primary and the secondary inductance is calculated by

$$L_{k.gap} = \frac{\mu_0 A_{core} N_k^2}{l_g + \frac{l_m}{\mu_{core}}} \quad k = 1, 2 \quad (2.40)$$

Finally, the required window area for a core with the target window utilization factor  $K_{cu.target}$  is given by [10]

$$K_{cu.target} = S_1 S_2 S_3 S_4 \quad (2.41)$$

where  $S_1$  depends on the insulation of the selected wire. According to [12], most insulation of litz wires are single or heavy build. Depending on the ratio of bare copper area and the whole wire area, heavy or single build are determined.  $S_2$  is wire lay or fill factor, depending on how the wires are wound.  $S_3$  is effective winding area factor.  $S_4$  is insulation factor and means window area that usable for insulation.

The obtained window utilization factor  $K_{cu.obtained}$  depends on real window area  $A_{w.effective}$  and winding area  $A_{winding}$ , i.e.,

$$K_{cu.obtained} = \sum_{k=1}^2 \frac{A_{winding.k}}{A_{w.effective.k}} \quad k = 1, 2 \quad (2.42)$$

$A_{w.effective}$  is sometimes specified in the core datasheet. Otherwise it can be estimated by [10]

$$A_{w.effective} = A_w S_3 \quad (2.43)$$

The core loss for an inductor is calculated by

$$P_{fe} = K_{fe} \cdot (B)^b \cdot f_{sw} \cdot A_{core} \cdot l_m \quad (2.44)$$

where  $K_{fe}$  is material coefficient, 24.7 for ferrite, and  $b$  also depends on material and kept to be 2.6 for ferrite.  $l_m$  is magnetic path length specified in the datasheet. However, some core manufacturers provides core losses as a function of operating frequency. For instance, at a switching frequency of 50[kHz] with VITROPERM material in blue color, core loss is 150W.

Copper losses are calculated by

$$P_{cu} = \sum_{k=1}^2 R_{winding.k} \cdot I_{k.rms}^2 \quad (2.45)$$

where  $R_{winding}$  is calculated by

$$R_{winding} = \rho_{wire} \frac{l_{wire}}{N_{wire.bundle} A_{wire}} \quad (2.46)$$

where  $\rho_{wire}$  is resistivity of the selected wire,  $l_{wire}$  is wire length calculated by (2.32) and  $N_{wire.bundle}$  is the number of wires in one bundle calculated by (2.31).

After both core and copper losses are found, the temperature rise in degree Celsius in the transformer can be found by using [10]

$$T_{rise} = 450 (\text{Wattdensity})^{0.826} \quad (2.47)$$

where (Wattdensity) is  $\frac{P_{fe}+P_{cu}}{A_{surface}}$ .  $A_{surface}$  is surface area of the core.

In order to make sure that the peak flux density in the core exceed saturation flux density specified in the core datasheet, The peak flux density is calculated by

$$B_{peak} = \frac{N_1 (I_1 + \frac{\Delta i_{L,1}}{2})}{(\frac{l_g}{\mu_0} + \frac{l_m}{\mu_0 \mu_{core}})} - \frac{N_2 (I_2 + \frac{\Delta i_{L,2}}{2})}{(\frac{l_g}{\mu_0} + \frac{l_m}{\mu_0 \mu_{core}})} < B_{sat} \quad (2.48)$$

where the minus sign indicates that the direction of the output current is from the transformer side to the load side. It can be seen from (2.58) that  $B_{peak}$  is highest when the airgap is zero.

$\Delta i_L$  in transformer is calculated based on the inductance of the primary and the secondary turns, and the maximum value is taken by using  $D_{max}$ .

$$\Delta i_{L,k} = \frac{D_{max} V_k}{L_k f_{sw}} \quad (2.49)$$

### 2.4.2 Inductor design for nonisolated converters

An inductor is used to store energy to boost converters to step up the output voltage from the input voltage.

The copper loss for an inductor is calculated by

$$P_{cu} = I_{Lrms}^2 R_{winding} \quad (2.50)$$

where  $R_{winding}$  is calculated by (2.46).

The inductor rms current  $I_{Lrms}$  is calculated with

$$I_{L,rms} = \sqrt{I_{in}^2 + \frac{\Delta I_L^2}{12}} \quad (2.51)$$

where  $\Delta i_L$  is the estimated current ripple and it is kept to 20-30% of the input current for the boost converter in this thesis to obtain the inductance  $L$  value.

Core losses can be calculated by (2.44).

Due to the boost inductor, the diode peak current is the same as the peak value of inductor current  $I_{L,max}$  and calculated by

$$I_{L,max} = I_{in} + \frac{\Delta i_L}{2} \quad (2.52)$$

## 2. Theoretical Background

---

here  $I_{in}$  is also a value of total input current divided by the number of phases  $N_{ph}$  for a boost converter.

The number of turns  $N$  for a boost inductor is selected in such a way that it does not exceed saturation flux density, does not exceed core winding area, and at the same time has a lesser air gap to reduce fringing effect. As a rule of thumb, the air gap length is a tenth of core thickness  $h_{core}$ .

$$I_{C.rms} = \sqrt{\frac{(I_{in}(1-D))^2 D}{f_{sw}} + (I_{Lmin} + \frac{\Delta i_L}{2})^2 \frac{(1-D)}{f_{sw}}} \quad (2.53)$$

The air gap length  $l_g$  for a core is calculated in meter by

$$l_g = \frac{\mu_0 A_{core} N^2}{L} - \frac{l_m}{\mu_{core}} \quad (2.54)$$

Since the airgap is introduced, the fringing flux should be considered by using fringing flux factor  $F$ ,

$$F = 1 + \frac{l_g}{A_{core}} \ln\left(\frac{2G}{l_g}\right); \quad (2.55)$$

where  $G$  is winding length. For instance, if a bobbin is used, the height of the bobbin is  $G$ .

The new number of turns with the fringing effect considered is calculated by

$$N_{new} = \sqrt{\frac{l_g L}{\mu_0 A_{core} F}} \quad (2.56)$$

Thus,  $L_{new}$  the inductance with the fringing flux effect is calculated by

$$L_{new} = \frac{N_{new}^2 F}{\frac{l_g}{\mu_0 A_{core}} + \frac{l_m}{\mu_{core}}} \quad (2.57)$$

where  $l_m$  being magnetic path length in the core datasheet.

In order to make the flux density  $B$  remain less than saturation flux density  $B_{sat}$ , peak value of flux density  $B_{peak}$  is calculated by

$$B_{peak} = \frac{\mu_0 N_{new} (I_{in} + \frac{\Delta i_L}{2})}{l_g + \frac{l_m}{\mu_{core}}} < B_{sat} \quad (2.58)$$

The temperature rise in degree Celsius in the inductor can be found by (2.47).

### 2.4.3 Core selection

A transformer core is selected in such a way that it is not saturated and still have high flux density with relatively low frequency for less switching losses.

Also, the core window area  $A_w$  should be large enough to accommodate windings for both inductors and transformers, meaning that it has to have a proper window utilization factor.

The window utilization factor  $K_{cu}$  is the ratio between the effective winding area and core window area and calculated by (2.41).

The specifications for the core candidates are listed in Table 2.1.

**Table 2.1:** Core specification

	<b>B core</b>	<b>A core</b>	<b>C core</b>
<b>part number</b>	T60102-L2198-W160	T60004-L2160-W758	F1AH1266
<b>shape</b>	C	toroid	C
<b>flux density [T]</b>	0.3	0.3	0.1
<b>saturation flux density [T]</b>	1.2	1.2	1.23
<b>length [mm]</b>	198	-	173.4
<b>width[mm]</b>	115	-	101.4
<b>outer diameter[mm]</b>	-	160	-
<b>height(thickness) [mm]</b>	31.6	25	34
<b>window length [mm]</b>	118	-	106
<b>window width [mm]</b>	38	-	35
<b>inner diameter[mm]</b>	-	110	-
<b>core area[mm<sup>2</sup>]</b>	4484	9503.3	3604
<b>effective winding area[mm<sup>2</sup>]</b>	-	3250	-
<b>magnetic path length [mm]</b>	432	424	415
<b>core mass [kg]</b>	2.52	1.48	2.842
<b>permeability</b>	22000	22000	10000

The core candidates A and B are manufactured by vacuumschmelz made of VITROP-ERM 500[9] and C by Hitachi Metals made of amorphous [11].

### 2.4.4 Wire selection

The wires are selected to have high current density, less skin effect. Thus, originally a Litz wire is chosen from BLOCK.

The reason Litz wires are selected is that this prevents having a large impact from the skin effect. Skin effect occurs when alternating current with high frequency flows through a wire. At high frequency, eddy current is induced in the wire and it prevents the current from flowing deep in the core. Thus, the current is flowing through a surface of the wire,

## 2. Theoretical Background

---

resulting in high resistance in the wire and voltage drop, since the resistance of a conductor depends on its cross-section area.

It is recommended that Litz wire size in American Wire Gauge (AWG) is to be selected depending on switching frequency [13] [14]. If the operating frequency is 50kHz, it is recommended to use 36 to 38 AWG, of which the wire area is  $0.00797mm^2$  [15].

The specification of wire candidates are listed in Table 2.2.

**Table 2.2:** Wire specification

	<b>A wire</b>	<b>B wire</b>	<b>C wire</b>	<b>D wire</b>
<b>part number</b>	CLI 200/120	CLI 200/90	CLI 200/15	CUL 100/0.1
<b>cross section area [mm<sup>2</sup>]</b>	0.943	0.707	0.118	0.0079
<b>rated current [A]</b>	3.36	2.52	0.42	0.03
<b>current density [A/mm<sup>2</sup>]</b>	3.5631	3.5644	3.5593	3.8197
<b>volume density [kg/m<sup>3</sup>]</b>	8837	8837	8837	11130

The size of litz wires can be seen from their part names, e.g., when they have the name of N/XX, N is the number of strands and XX is the wire gauge [12]. The wire insulation type, whether it is single or heavy, can be seen from the N, the number of strands.

For instance, CUL 100/0.1 indicates that the number of strands are 100. The bare copper area for each AWG is given as well as the ratio of bare area over single  $\frac{A_{cu.bare}}{A_{singlebuild}}$  and bare area over heavy  $\frac{A_{cu.bare}}{A_{heavybuild}}$  are listed in [10]. For AWG 35,  $\frac{A_{cu.bare}}{A_{heavybuild}}$  is 0.698 and  $A_{cu.bare}$  is  $0.000056mm^2$ . Thus,  $100 \frac{0.000056}{0.698}$  gives  $0.008mm^2$ . Since the cross section area of CUL 100/0.1 is  $0.0079mm^2$ , it can be said that CUL 100/0.1 is heavy build type.

## 2.5 Pulse width modulation (PWM)

Switching of the MOSFET/IGBT can be controlled using Pulse width modulation. This can be done by generating switching signals using triangular waveforms  $V_{tri}$  and comparing them with the control voltage  $V_{control}$ . A general switching strategy can be seen in Figure 2.9.

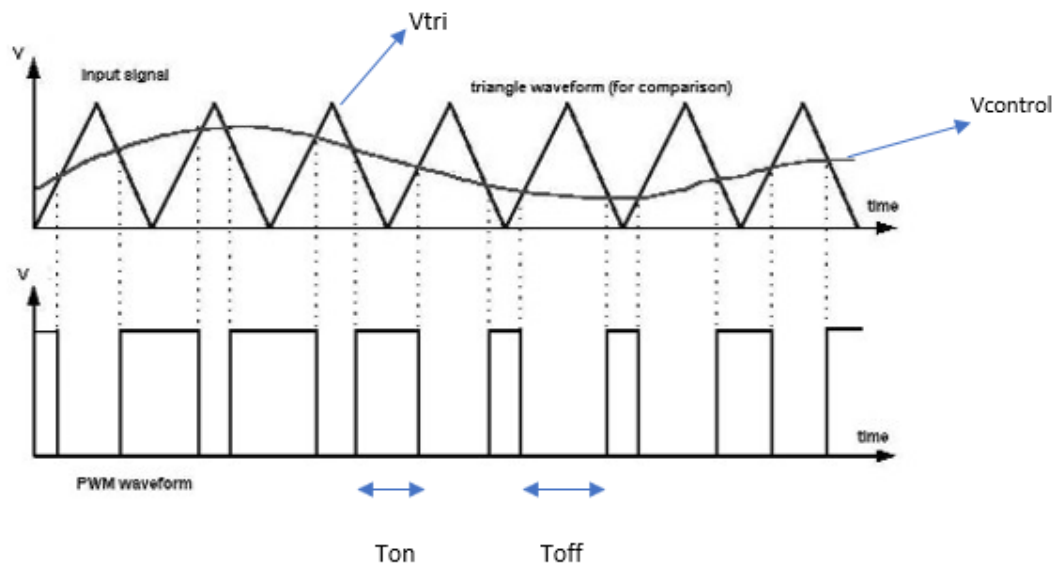


**Figure 2.9:** PWM control strategy

The output voltage for a particular switching frequency is controlled by varying  $V_{control}$ . This  $V_{control}$  affects the duty cycle hence the ON period  $t_{ON}$  and thus changes the output voltage [16]. The Duty cycle can be given by

$$D = \frac{t_{ON}}{T} = \frac{V_{control}}{V_{tripeak}} \quad (2.59)$$

Where  $T$  is the switching period.

## 2.6 Varying voltage drive system

The floating voltage system is a part of the research to be conducted. Here the whole system needs to be evaluated without the DC/DC converter. Mainly the schematic looks the same but the DC link is floating. The fuel cell stack and the battery are both connected to the DC link and the power flow is controlled by varying the internal impedance of the fuel cell stack. This is done by controlling the output characteristics of the fuel cell[5].

Analysis using a super capacitor as an auxiliary energy source has been done [5]. The higher energy density of a Super cap or a battery helps in providing the high peak transients of the load. This allows the fuel cell to operate at an average load power and thus flatter the profile of the fuel cell to extend the life time [5]. This thesis will be mostly focusing on using a battery as an auxiliary energy source.

## 2. Theoretical Background

---

# 3

## Case set-up

### 3.1 DC/DC converter design and simulation cases

The DC/DC converter topology will be simulated under two cases. Those two cases have only one difference: fuel cell stack characteristics. A Design A and an INN balance car will be simulated under conditions specified in Table 3.1, where the HV battery limit is the output voltage for the DC/DC converter.

**Table 3.1:** Simulation parameters-battery

	<b>values</b>
<b>HV battery limit</b>	252V-378V
<b>HV battery nominal</b>	324V
<b>drive system</b>	150kW (maximum)

The Design A will be simulated with design A while the INN balance car will be simulated with design B. Their electrical characteristics are specified below in Table 3.2.

**Table 3.2:** Simulation parameters-fuel cell stacks

	<b>Design A</b>	<b>INN balance car</b>
<b>input voltage [V]</b>	90-165	250-500
<b>input current [A]</b>	50-500	0-450
<b>maximum power [kW]</b>	45	100

The electrical characteristics of both designs are shown in Figure 3.1 and 3.2.

### 3. Case set-up

---

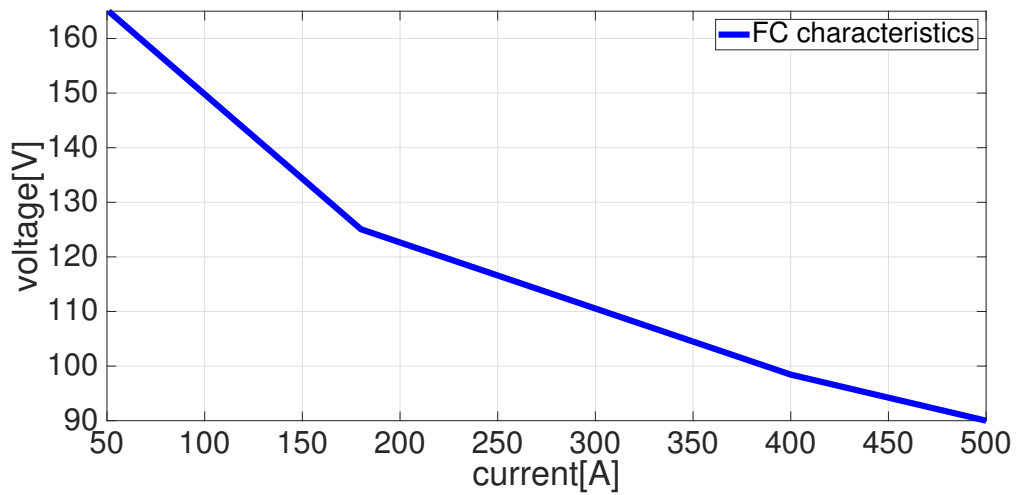


**Figure 3.1:** Fuel cell VI characteristics - Design A

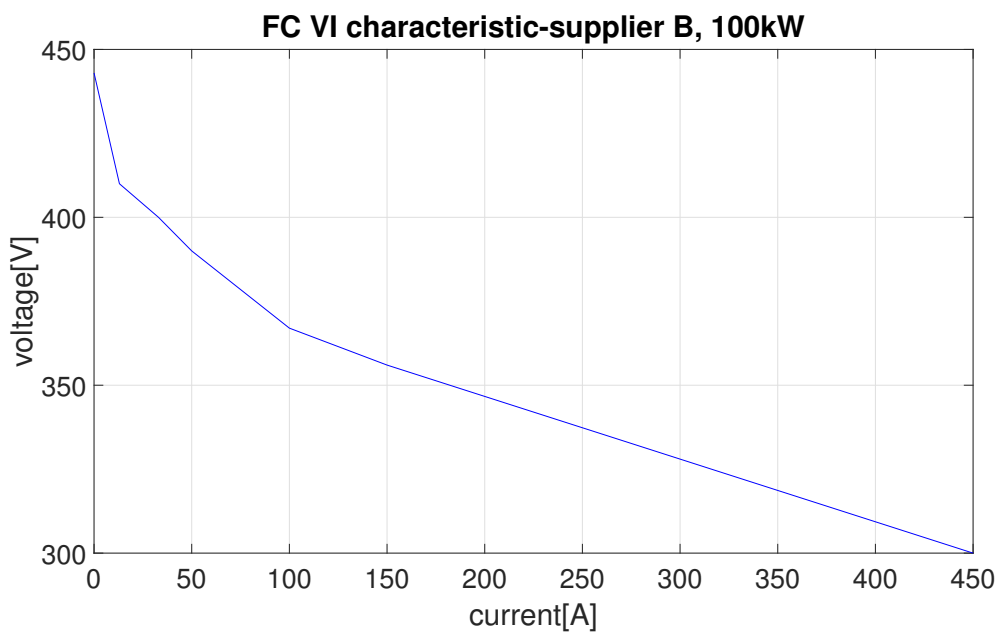


**Figure 3.2:** Fuel cell VI characteristics - Design B

These graphs are plotted using Matlab by using data provided from the manufacturer's datasheets.

## 3.2 Design A

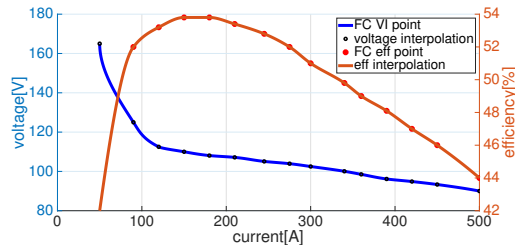


**Figure 3.3:** Fuel cell VI and efficiency characteristics - Design A

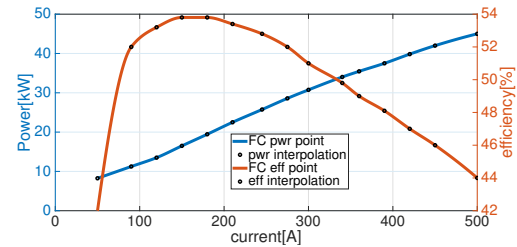


**Figure 3.4:** Fuel cell power and efficiency characteristics - Design A

Figure 3.3 and Figure 3.4 are redrawn for 45kW fuel cell stack by scaling the values of the 30kW graph. The red and the blue in Figure 3.3 indicate fuel cell stack efficiency and voltage as function of current. The red and the blue in Figure 3.4 indicate fuel cell stack efficiency and fuel cell stack power as function of current.

Topology selection processes, components selection and base verification regarding the Design A parameters specified in Table 3.1 and Table 3.2 will be written in this section.

### 3.2.1 DC/DC Converter topology selection process for design and simulation

A high voltage DC/DC converter described in Figure 2.4 for a prototype fuel cell vehicle will be designed and simulated for its circuit behavior and size.

Since maximum 378V will be used on the output side of the DC/DC converter, isolation between the fuel cell and the inverter is selected initially. Then, several topology of the DC/DC converter, such as Figure 2.5, Figure 2.6, Figure 2.7 and so on, will be investigated to obtain high efficiency, safety, small size, light weight, low cost.

primary	efficiency	cost (# components)	max Pout	Volume	raw score	weighted score
weighting	4	3	1	2		
half-bridge	3	2	1	3	9	25
full-bridge	2	1	3	3	9	20
push-pull	2	3	3	1	9	22
higher score	higher	lower	higher	smaller		

**Figure 3.5:** Value analysis chart - primary side

### 3. Case set-up

secondary	efficiency	cost (# components)	Volume	raw score	weighted score
weighting	3	2	1		
fullwave bridge	2	1	2	5	8
center tap	1	2	1	4	8
higher score	higher	lower	smaller		

**Figure 3.6:** Value analysis chart - secondary side

In Figure 3.5 and Figure 3.6, both the primary side and secondary side of the DC/DC converter are scored with weightings. For Figure 3.5, since three topology were selected, the highest score is three and the lowest is one. For Figure 3.6, the highest score is two while the lowest is one.

The weighted core shows that half-bridge scored highest for the primary side while both full-wave bridge and center tap were highest for the secondary side. However, due to high power and design limitations of center tap, the full bridge and full wave bridge topology is selected for the design.

To compare the cost, volume, and efficiency, non-isolated topologies will be designed as well. The decision is made by the similar value analysis chart in Figure 3.7.

non-isolated	efficiency	cost(# components)	volume	max Vout	raw score	weighted score
weighting	4	1	2	3		
boost	2	4	1	1	8	17
cascaded boost	1	2	2	3	8	19
three level boost	3	3	3	2	11	27
cascaded three level boost	4	1	4	4	13	37
higher score	higher	lower	smaller	higher		

**Figure 3.7:** Value analysis chart - boost converters

The cascaded three-level boost converter scored highest in Figure 3.7 [17]. On the other hand, maximum 0.7619 of duty cycle, which is less than 0.9 meaning that it does not require sophisticated control and is not considered to be too high conversion ratio, is required in this application [18]. Thus, the three-level boost converter is selected for a non-isolated converter for the Design A for comparison. However, due to its simplicity, a three phase boost converter, which is three basic boost converters connected in parallel with phase shifts, is selected for design.

A dual active bridge is used when there is a need for power flow from both the input to the output and/or output to the input as can be seen in Figure 2.2, Case II. In case of dual active bridge, the diodes on the secondary of the full bridge are replaced by MOSFETs. The advantage of having MOSFETs on both sides is that soft switching is possible so the power loss is reduced. However, it can cause unwanted current flow into the primary side. The cost difference is shown further in the analysis part.

### 3.2.2 DC/DC converter components selection for simulation and volume packaging

After selecting the DC/DC converter topology, its components are selected as per the requirements shown in Table 3.1 and Table 3.2.

#### 3.2.2.1 Component rating selection

In order to select components, it is necessary to know component ratings not to over and/or underdimension the components. Overdimension causes high cost, volume and weight while underdimension causes malfunctioning of a system.

The ratings of the components will be calculated by using MATLAB. First, for the isolated converter, under different conditions mentioned in Table 3.3, a transformer turns ratio will be selected. Then, output voltage as function of duty cycles (from 0.1 to 0.5) will be calculated to observe operation range. Also, transformer will be designed to have high efficiency and low volume. Then the component ratings for both input and output side will be determined.

The same process applies for non-isolated converters. The duty cycle for this type of converters has maximum and minimum duty cycles fixed by input and output voltages as written in (2.23). For non-isolated converters, inductors will be designed instead of transformers.

In addition, several converters connected in parallel will be calculated to reduce current ratings for the MOSFETs and diodes. The reason is that during the base market search, MOSFETs with 500A current ratings were found to be rare. But to have a simpler control different number of converters are used instead of having several parallel MOSFETs. This also helps in reducing the current ripple on the output.

#### 3.2.2.2 Transformer selection

A transformer for the DC/DC converter isolation will be calculated with MATLAB as well. First, the number of turns, turns ratio, the primary and the secondary inductance values will be obtained. Initial values for calculating the transformer are specified in table 3.3.

**Table 3.3:** DC/DC converter parameters for transformer design

DC/DC converter	case I	case II	case III
<b>input /output voltage</b>	90V / 378V	90V / 378V	90V / 378V
<b>input / output current</b>	500A / 116.67A	500A / 116.67A	500A / 116.67A
<b>switching frequency</b>	20kHz	50kHz	100kHz
<b>input power</b>	45kW	45kW	45kW
<b>target efficiency</b>	99%	99%	99%

The difference between three cases in Table 3.3 is only switching frequencies. This is because higher switching frequency results in lower volume with lower efficiency.

Secondly, the real voltage and current under the conditions will be obtained in accordance with the initial core and wire on the market. Initially, for the fuel cell stack for Design A, the transformer core is manufactured by Vacuumschmelze and listed in Table 2.1. These are vitroperm 500, nanocrystalline cut cores.

When it comes to wire, a Litz wire is selected to reduce skin effect and proximity effect which causes further losses. Wire sizes are selected in accordance with the switching frequency. Wires are also listed in Table 2.2.

#### 3.2.2.3 Inductor selection

The inductor for the boost converter will be designed in the similar way to transformer. Also, the same core and the same wire as the transformer, which are in Table 2.1 and in Table 2.2, will be used for the initial design.

In this case, the inductor value is less but has to withstand high current. Thus, an air gap is introduced to reduce inductance and peak flux density for the same current to avoid saturation. The air gap is designed based on (2.54).

#### 3.2.3 Base verification

The base verification is carried out by SIMULINK. For the base verification, the MOS-FETs and Diodes are selected to withstand peak voltage and current through them. Load resistors are selected to have desired power output and voltage by the equation according to.

$$R_{load} = \frac{V_{desired.out}^2}{P_{in}} \quad (3.1)$$

When it comes to design,  $V_{desired.out}$  is selected to be 378V which is the maximum high voltage battery voltage.  $P_{in}$  is 45kW for the Design A.

##### 3.2.3.1 Base boost converter

In Figure 3.8, a model of a base boost converter is shown.

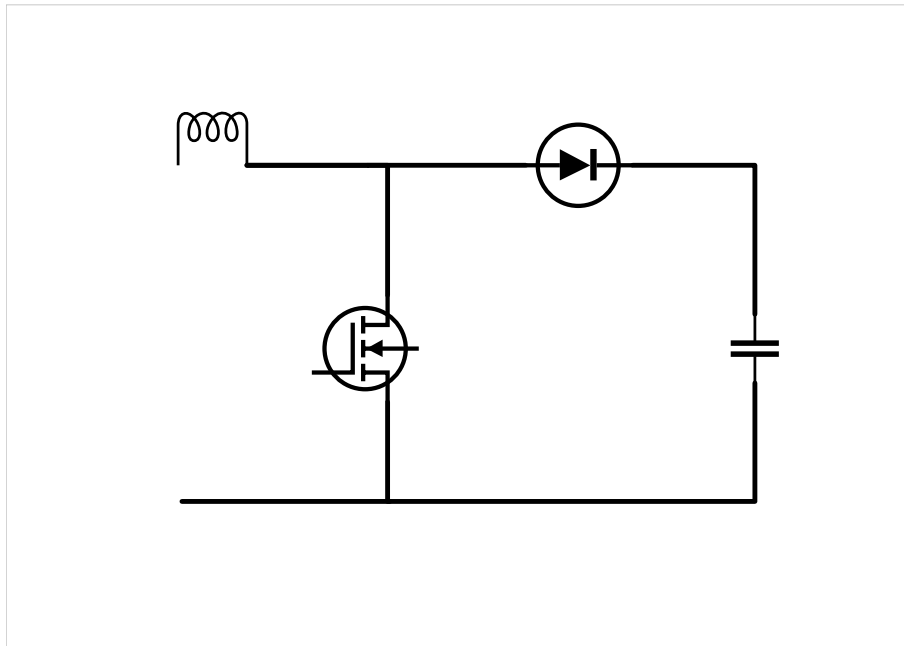


**Figure 3.8:** base boost converter

The input voltage is 90V and the duty cycle is the maximum duty cycle calculated by (2.23), 0.76 and the load resistor is calculated by (3.1), 3.1752. Inductors and capacitors are selected by (2.24) and (2.14).

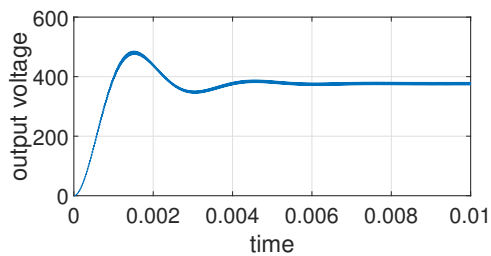


**Figure 3.9:** Output voltage-boost converter

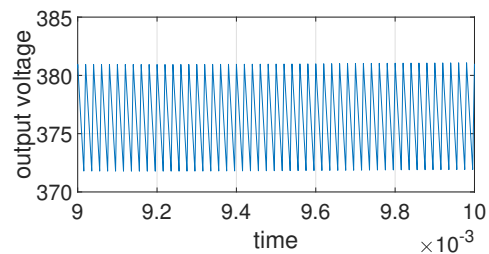


**Figure 3.10:** Output voltage ripple-boost converter

It is shown that the output voltage is 376V in Figure 3.9 with 12V of a peak to peak ripple in Figure 3.10.

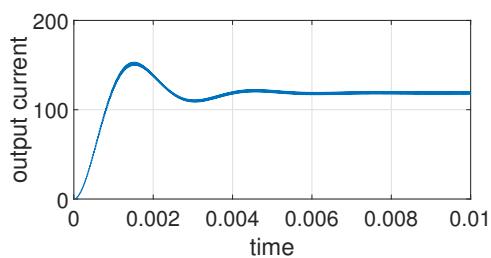


**Figure 3.11:** Output current-boost converter

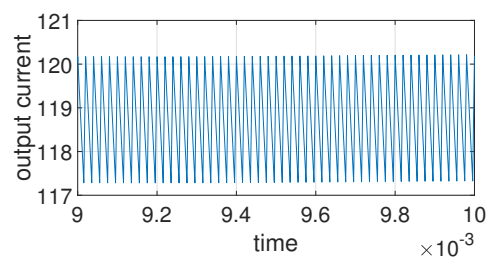


**Figure 3.12:** Output current ripple-boost converter

### 3. Case set-up

---

It is shown that the output current is 118.5A in Figure 3.11 with 3.6A of the peak to peak ripple in Figure 3.12.

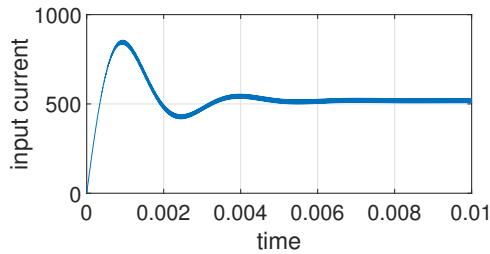


**Figure 3.13:** Input current-boost converter

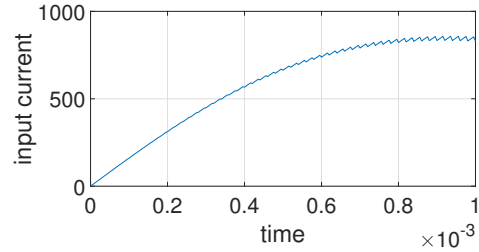


**Figure 3.14:** Input peak current-boost converter

It is shown that the average input current is 500A in steady state in Figure 3.13 with 1600A of the peak in Figure 3.14.

#### 3.2.3.2 Full bridge converter with two legs

In Figure 2.5 and Figure 2.6, a model of a fullbridge converter with two legs is shown separately.

Switching frequency is selected to be 50[kHz].

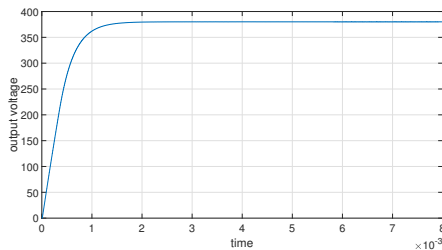


**Figure 3.15:** Output voltage-with 2 legs

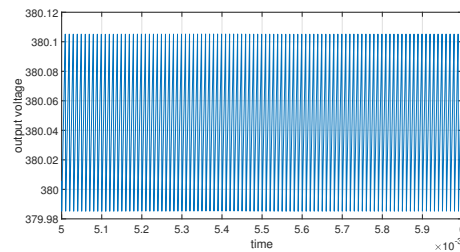


**Figure 3.16:** Output voltage ripple-with 2 legs

In Figure 3.15 and Figure 3.16, output voltage and voltage ripple are shown, respectively.

### 3.3 Comparison with varying voltage system

It is noticed that the system with the DC/DC converter is able to supply more stable voltage to the load as compared with the fuel cell car system without a DC/DC converter.

## 3.4 INN balance car

This section discusses the use of another DCDC topology for a fuel cell of capacity 100kW.

### 3.4.1 Simple buckboost converter

This section just shows base verification of the simple buck boost. The duty cycle of 0.55 for which the output parameters are shown is a chosen value to get the maximum DC link voltage.

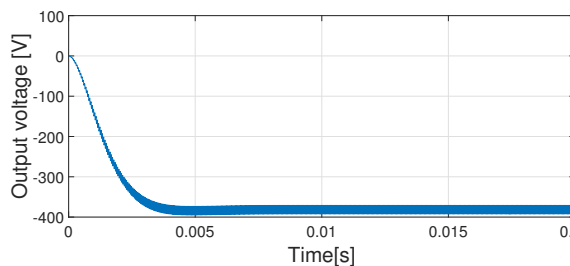


**Figure 3.17:** Output voltage of a buck boost converter

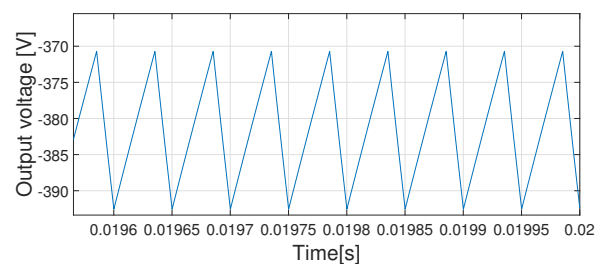


**Figure 3.18:** Output voltage ripple of a buck boost converter

The output voltage as seen in Figure 3.17 is 385 V and the ripple voltage from Figure 3.18 is 20 V peak to peak.

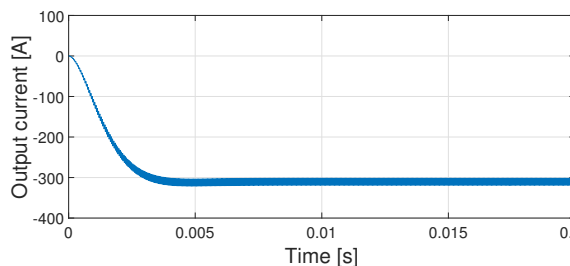


**Figure 3.19:** Output current of a buck boost converter

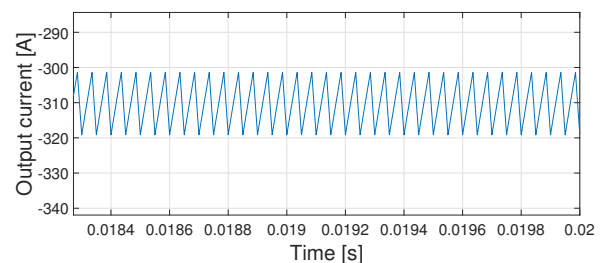


**Figure 3.20:** Output current ripple of a buck boost converter

The average output current as seen in Figure 3.19 is 315 A and the ripple current from Figure 3.20 is 16 A peak to peak.



# 4

## Analysis

### 4.1 Design A

For the initial calculation and simulation, an over-dimensioned MOSFET and diode available on the market are used and their specifications can be seen in Table 4.1.

**Table 4.1:** Specification of MOSFET and diode for initial calculation

	<b>MOSFET</b>	<b>Diode</b>
breakdown voltage [V]	170	1600
max continuous current [A]	-	350
average continuous current [A]	220	-
forward voltage drop [V]	-	1.5
on resistance [ $m\Omega$ ]	6.3	4.3

#### 4.1.1 Isolated Full bridge - full wave unidirectional DC/DC converter

This section is about the design and simulation of an isolated full-bridge converter. The efficiency of the converter will be put forth and simulation of it will be shown. Then cost and volume analysis follow.

##### 4.1.1.1 Loss calculation

The MOSFET losses as mentioned from (2.1) to (2.5) are calculated and the results with a minimum input voltage of 90V in Table 3.1 and a maximum output voltage 378V in Table 3.2 for a single converter are listed in Table 4.2. For other calculations later, a minimum input voltage of 90V and a maximum output voltage 378V will be used as well.

**Table 4.2:** Loss values for a single converter with initial components at 50kHz

Type of loss	Value[Watt]
MOSFET conduction	688.38
MOSFET switching	343.01
MOSFET dead time	58.801
total MOSFET	4361.5
diode conduction	73.06
diode switching	8
diode off time	43.047
total diode	496.43
L filter	4.3785
C filter ceramic	53 $\mu$
C filter electrolyte	0.03
total copper	2.4
total core	37.8
input power	45000
output power	39350
efficiency	88.9

According to Table 4.2, the efficiency is 88.9%. This efficiency is just one point, not the average value nor the peak value. The total efficiency is shown in Figure 4.1 and Figure 4.2. The efficiency in Table 4.2 is the cross section of the black dotted line and the blue line in Figure 4.1, and also the black "o" mark on the blue line in Figure 4.2.

In Figure 4.1 and Figure 4.2, the efficiencies as function of output voltages and output powers with different input voltages are shown. For both figures, magenta color means having a minimum output voltage, 252V, and black color means having maximum output voltage, 378V.

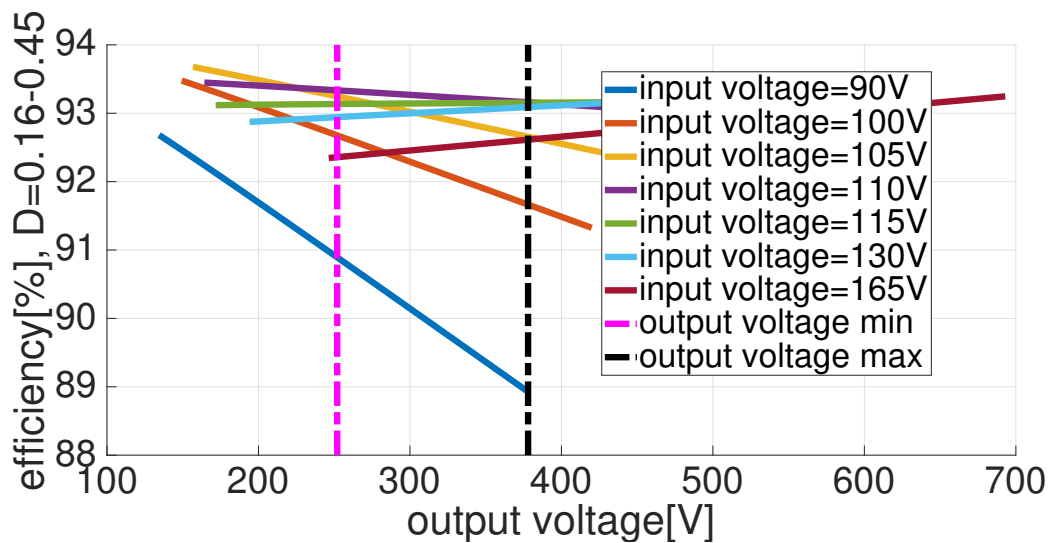


**Figure 4.1:** Output voltage and efficiency with 2 legs, 1 converters in parallel

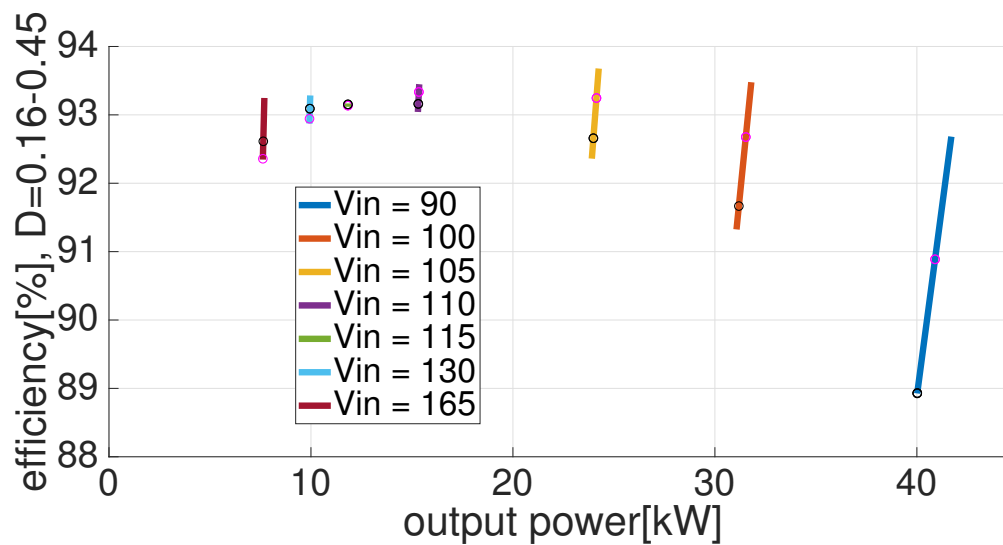


**Figure 4.2:** Output power and efficiency with 2 legs, 1 converters in parallel

These graphs show the characteristics of the fuel cell as a low voltage and high current power source. In Figure 4.2, it can be noticed that having low input voltages results in higher output powers and lower efficiencies. This is because when the fuel cells supply a low input voltage, the current from them is high, as can be seen in Figure 3.3. Having high current results in high losses, thus lower efficiency is obtained.

In addition, the efficiency at maximum output voltage, magenta o mark in Figure 4.2 and the one at minimum output voltage, black "o" mark in the same figure becomes reverse as input voltage increases. When the fuel cells supply an input voltage of 90V, having maximum output voltage results in lower efficiency than having minimum output voltage. The efficiency range is wide as well. As the input voltage increases, the efficiency range decreases till the input voltage reaches 115V.

From an input voltage higher than 115V, the efficiency at maximum output voltage is higher than the one at minimum output voltage and the efficiency range starts increasing.

To find the optimized total efficiency, calculation with multiple converters in parallel is conducted with MATLAB and the results are shown in Table 4.3 below.

**Table 4.3:** Loss values for multiple converters in parallel

<b>loss[W]/number of converters</b>	<b>2</b>	<b>3</b>	<b>4</b>
MOSFET conduction per unit	172.1	76.5	43.023
MOSFET switching per unit	171.5	114.34	85.75
MOSFET dead time per unit	29.401	19.6	14.7
total MOSFET loss	2985.6	2527.5	2298.8
diode conduction per unit	37.8	25.5	19.2
diode switching per unit	8	8	8
diode off time per unit	43.05	43.05	43.05
total diode loss	710.69	918.24	1124.1
L filter	4.4	4.4	4.4
C filter ceramic	53 $\mu$	53 $\mu$	53 $\mu$
C filter electrolyte	0.03	0.03	0.03
total copper	12	35.375	79.0
total core	151.2	340.2	604.8
input power	45000	45000	45000
efficiency	91.3	91.4	90.71

The only difference in Table 4.3 is the number of converters while the number of MOSFETs is kept to four in this case. Having more than one converter means that the same number of transformers are needed, which led to packaging issues and controls of switches become complicated as well. Therefore, it is required to find the optimized number of converters for easy packaging and simpler control.

Comparing Table 4.2 with Table 4.3, it is noticed that having one converter and two converters have 2% of the difference in efficiency. This means 900W of power can be saved when having one more converter in parallel.

Comparing two converters in parallel and three converters in parallel, the difference in efficiency is only 0.1%, meaning that 45W is lost only when having one more converter. Thus, having two converters is optimum, not considering component ratings, costs and volumes.

The result from the multiple MOSFET cases with two converters in parallel is shown in Table 4.4. This is calculated to check how much efficiency can be obtained when having complex control.

**Table 4.4:** Loss values for multiple MOSFETs in parallel with two converters

<b>loss[W]/number of MOSFET legs</b>	<b>2</b>	<b>4</b>
number of MOSFETs	8	16
MOSFET conduction per unit	172.1	43.02
MOSFET switching per unit	171.5	85.75
MOSFET dead time per unit	29.401	14.7
total MOSFET loss	2985.6	2298.8
diode conduction per unit	37.8	38.42
diode switching per unit	8	8
diode off time per unit	43.05	43.05
total diode loss	710.69	715.73
L filter	4.4	4.4
C filter ceramic	53 $\mu$	53 $\mu$
C filter electrolyte	0.03	0.03
total copper	12	12
total core	151.2	151.2
input power	45000	45000
efficiency	91.3	92.81

It is seen from Table 4.4 that having more legs results in higher efficiency. From having two legs, which is minimum, to four legs, the efficiency is increased by 1 %, i.e., 450W of power is saved.

Another advantage of having more MOSFET legs is that each MOSFET can have lower current ratings, meaning that cost and volume of each MOSFET are decreased while the efficiency is increased. However, having more legs also means the total volume and cost of MOSFETs are increased as well. Since heat sink for the MOSFETs are inevitable partly due to high ambient temperature in the box, 85° C, and due to high power consumption in MOSFETs, more MOSFETs result in more heat sinks, increasing the total volume.

The whole efficiency graphs as function of output voltage and output power are shown in Figure 4.3 and Figure 4.4, respectively.

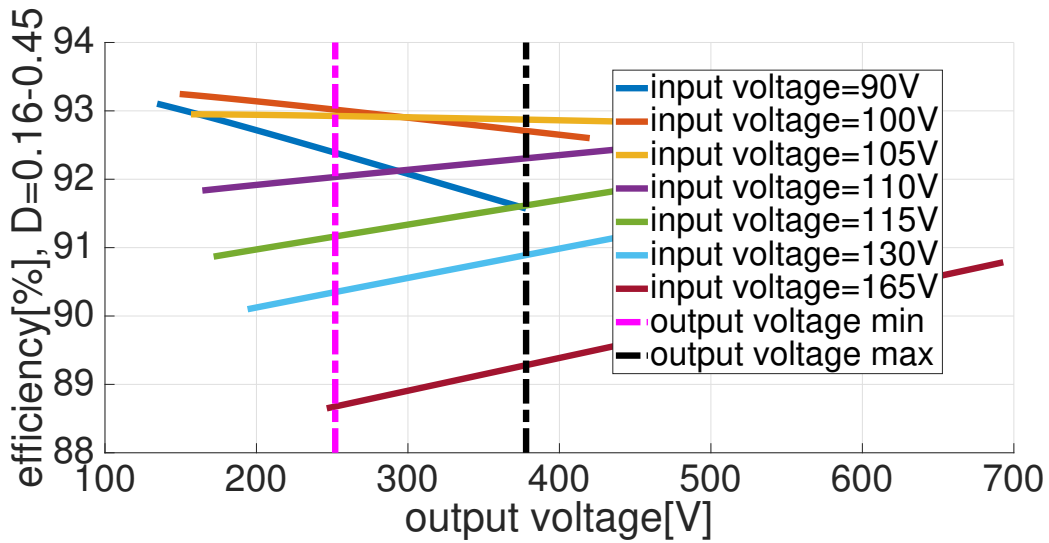


**Figure 4.3:** output voltage and efficiency with 2 legs, 2 converters in parallel

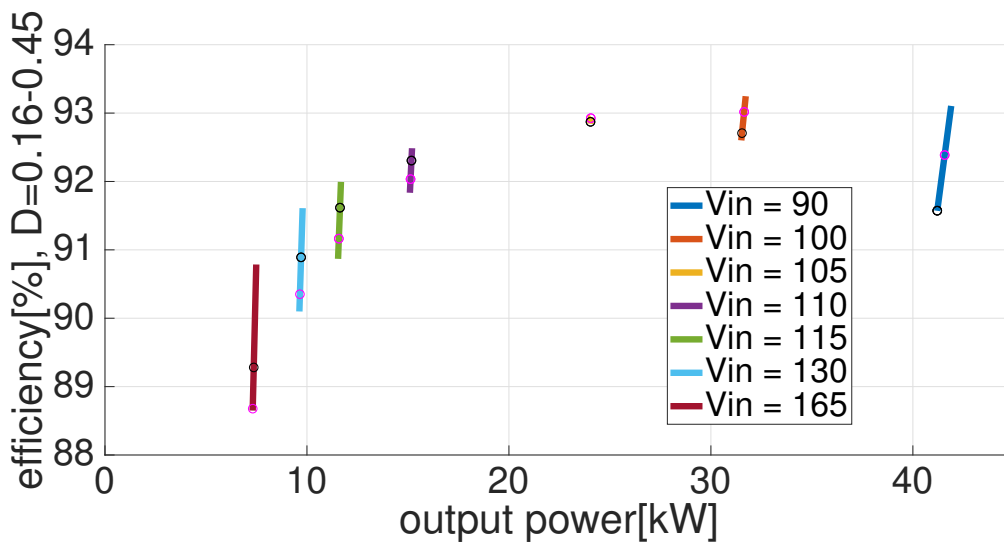


**Figure 4.4:** output power and efficiency with 2 legs, 2 converters in parallel

In Figure 4.4, it is noticed that the worst case scenario, where the output voltage is 378V when the input voltage is 90V, has a higher efficiency than the cases where the input voltage is higher than 110V.

It is also noticed that after an input voltage of 105V, the efficiency at the maximum output voltage starts being higher than efficiency at an minimum input voltage. In Figure 4.2, this phenomenon starts at input voltage of 115V. Thus, the efficiency variation for the output power range is more stable for two converters in parallel.

Since the components in both figures are overdimensioned, the efficiency with two converters in parallel will increase more after cost analysis.

#### 4.1.1.2 Control strategy

The fuel cell needs to be operated only within a certain power range to ensure maximum power usage. So the current and voltage profile of the fuel cell and also the converter output is going to be studied. The voltage profile is going to be controlled through the CAN communication as mentioned in the case setup. The PWM module from the market for an existing PHEV/HEV's will be studied and suggestion for a better fit possible in the converter will be given.

The input and output parameters used to design the transformer such that maximum control of the duty cycle over the required voltage range is possible. The selected transformer has the voltage profile shown in Figure 4.5. In the figures,  $D$  implies duty cycle, magenta dotted line means normal operation range of HV battery specified in table 3.1, and black dotted line means HV battery limit specified in the same table.

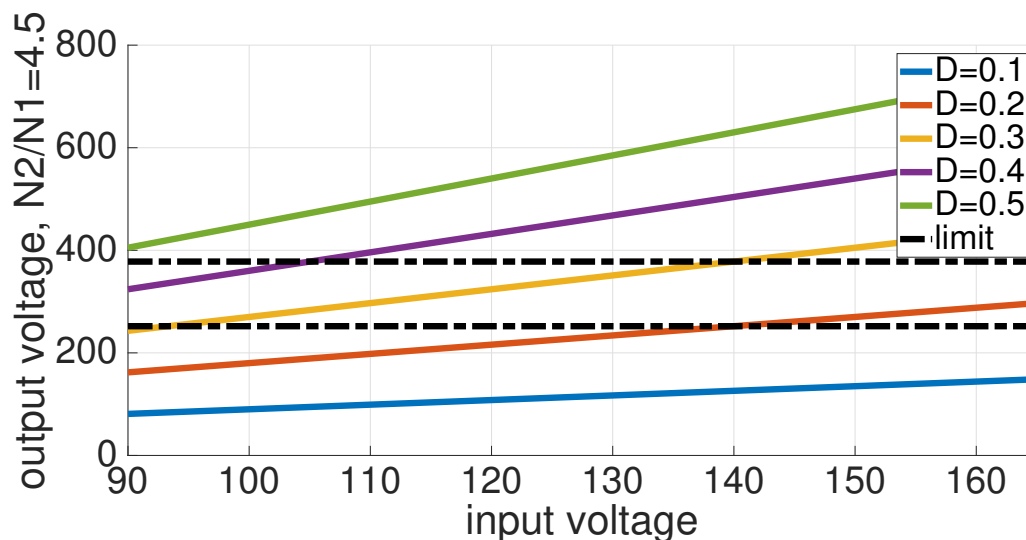


**Figure 4.5:** Duty cycle variation for the voltage profile with turns ratio of  $N = \frac{N_2}{N_1} = 4.5$

The input voltage varies between 90-165 V so the output voltage requirements at every input voltage level need to be satisfied by varying the duty cycle. In this case the transformer turns ratio of  $\frac{N_2}{N_1} = 4.5$  shows the widest duty cycle range when the duty cycle varies from 0.15 - 0.45, 0.5 being the limit in Figure 4.5.

#### 4.1.1.3 Transformer and wire setup for B core in Table 2.1

The initial design of one transformer for a single converter is calculated with the parameters: B core in Table 2.1, D wire in Table 2.2 and the case II in Table 3.3. The results are specified below in Table 4.5 and in Table 4.6.

**Table 4.5:** Result parameters for wire setup

Wire	primary	secondary	total
length [m]	0.31	1.21	-
number of wires per bundle	16667	3691	
number of turns	2	9	-
inductance [ $\mu\text{H}$ ]	203.51	4121	-
copper loss [W]	-	-	2.6
volume [ $\text{cm}^3$ ]	-	-	75.7
wire mass [kg]	-	-	0.8

**Table 4.6:** Result parameters for core setup

	values
switching frequency [kHz]	50
core loss [W]	37.8
target window utilization factor	0.37
real window utilization factor	0.2
Peak flux density	0.24
core mass [kg]	2.52
total mass [kg]	3.7

The MOSFET and diode losses are neglected in this case to see only the transformer loss. It is observed from Table 4.6 that the real window utilization factor is less than the target window utilization factor. This means that the space occupied by the winding is lower than the available winding space in the core. Thus this core can be used for this application or the smaller core can be found for further reducing the total volume.

The designed values for the two converters in parallel are shown in Table 4.7 and Table 4.8 with the same wire and the same core used for a single transformer in Table 2.1 and in Table 2.2. The values are listed per unit. Having two converters in parallel means that the current is divided into half.

**Table 4.7:** Result parameters for wire setup per unit

Wire	primary	secondary	total
length [m]	0.3	1.16	
number of wires per bundle	8334	1846	
number of turns	2	9	
inductance [ $\mu\text{H}$ ]	203.51	4121	
volume [ $\text{mm}^2$ ]			35.5
copper loss [W]			4.4
wire mass [kg]			0.4

**Table 4.8:** Result parameters for isolated converter per unit

	values
switching frequency [kHz]	50
core loss [W]	37.8
target window utilization factor	0.3717
real window utilization factor	0.1
core mass [kg]	2.52
total mass [kg]	5.83

In Table 4.8, the window utilization factor is 0.26, meaning that transformer window area can be smaller half with the same core area. Having a lower window area will also lead to lesser volume, and might lead to lower cost.

The same procedure is carried out with the A core in Table 2.1 and listed in Table 4.9 for wires and in Table 4.10 for cores in each converter.

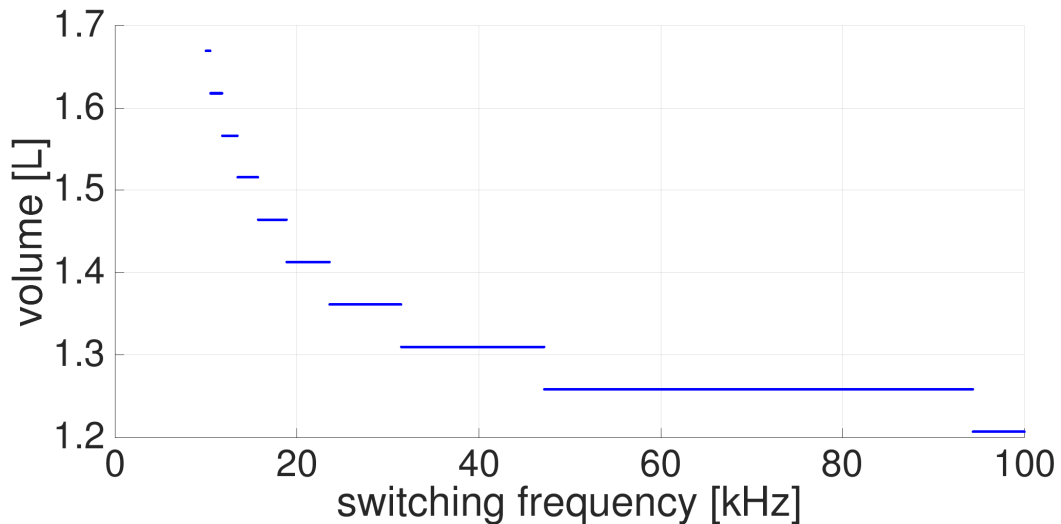
**Table 4.9:** Result parameters for wire setup for A core in Table 2.1

Wire	primary	secondary	total
length [m]	0.31	1.21	-
number of wires per bundle	16667	3691	
number of turns	4	17	-
inductance [ $\mu\text{H}$ ]	35	630	-
copper loss [W]	-	-	15.4
volume [ $\text{cm}^2$ ]	-	-	123
wire mass [kg]	-	-	1.37

**Table 4.10:** Result parameters for core setup for A core in Table 2.1

	<b>values</b>
switching frequency [kHz]	50
core loss [W]	22.2
target window utilization factor	0.37
real window utilization factor	0.2
Airgap length[cm]	0.025
Peak flux density	0.27
core mass [kg]	1.48
total mass [kg]	3

In Figure 4.6, total transformer volume as a function of different switching frequencies is shown.

**Figure 4.6:** Total transformer volume over switching frequency

It can be noticed that the total volume for transformers and wires for two converters and two legs of the MOSFETs is decreased by 10% from 20kHz to 50kHz, i.e. from 1.4L to 1.26L. The total volume is decreased by 5% from 50kHz to 100kHz, i.e. from 1.26L to 1.2L. Having a higher switching frequency leads to higher switching losses. The efficiency comparison between 20kHz, 50kHz, and 100kHz is in Table 4.11.

**Table 4.11:** Loss values of a two full bridge isolated converter in parallel for different frequencies

	<b>20kHz</b>	<b>50kHz</b>	<b>100kHz</b>
<b>efficiency [%]</b>	83	91.4	88.7

It is seen from Table 4.11 that 8% efficiency is increased from 20kHz to 50kHz whereas 4% efficiency is decreased when increasing the frequency from 50kHz to 100kHz.

It is said that the efficiency is higher with the lower frequency. However, in this case, the lower the frequency, the higher the number of turns, leading to higher copper losses.

Compared to using a switching frequency of 50kHz, using a switching frequency of 20kHz loses efficiency of 8% and 10% of volume while using switching frequency of 100kHz loses efficiency of 4% and gains 5% of volume. Thus, 50kHz is more suitable for this application.

#### 4.1.1.4 Simulation

A single phase basic simulation model of an isolated full bridge in LTspice was developed as seen in Figure 4.7. The components are selected from the available ones in LTspice and were later replaced with the LTspice model of the components closely resembling the required values. However, issues involving higher simulation time and the real MOSFET model for the required specifications resulted in that the simulations were done in SIMULINK.

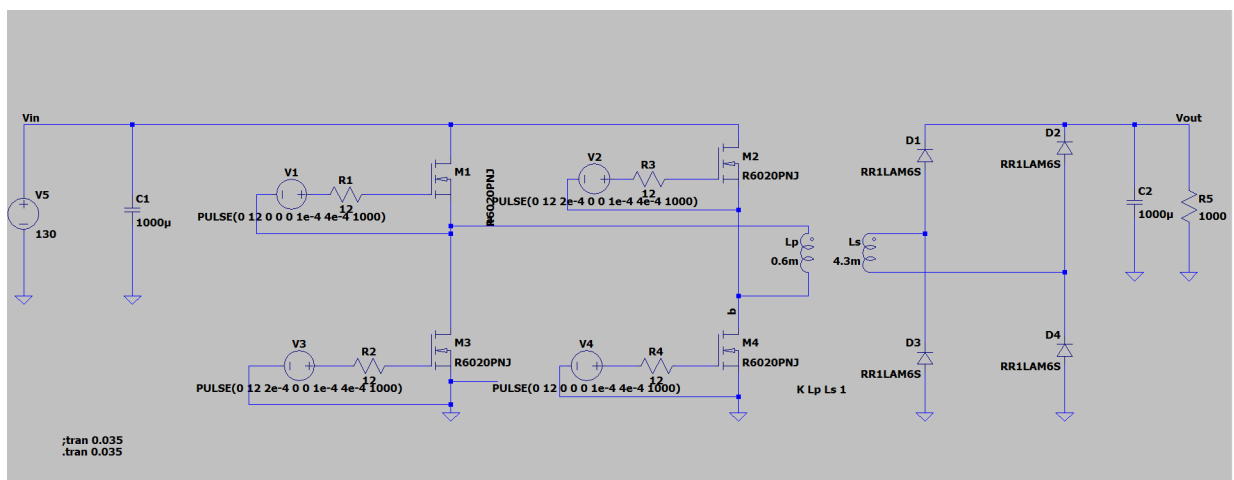


**Figure 4.7:** Initial circuit model of full bridge DC/DC converter in LTspice

The simulation time in Figure 4.7 is 35 ms and the time delay between M1 M4 and M2 M3 is 0.03 ms. The switching frequency is 10 kHz which is chosen for the initial design of the transformer dimension and the high power requirement. The input voltage is the nominal value of 130 V and based on the transformer design, the output voltage is expected to be near to 324 V i.e., the nominal output voltage. Also, the transformer is considered perfectly coupled i.e. without any leakage inductance.

The simulation model in Figure 4.8 is an isolated full bridge converter(2 converters in parallel) with four legs in Simulink. The secondary side is shown in Figure 2.6.

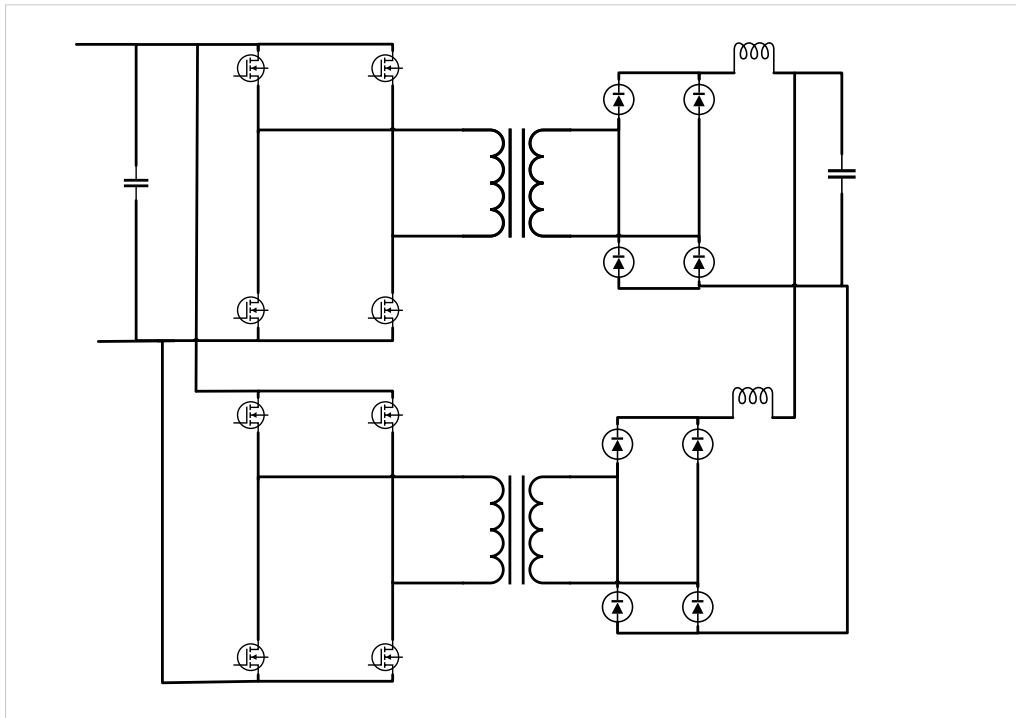


**Figure 4.8:** Isolated fullbridge converter with 2 phases and 2 MOSFET legs

It is simulated to verify the current to MOSFETs and output voltage.

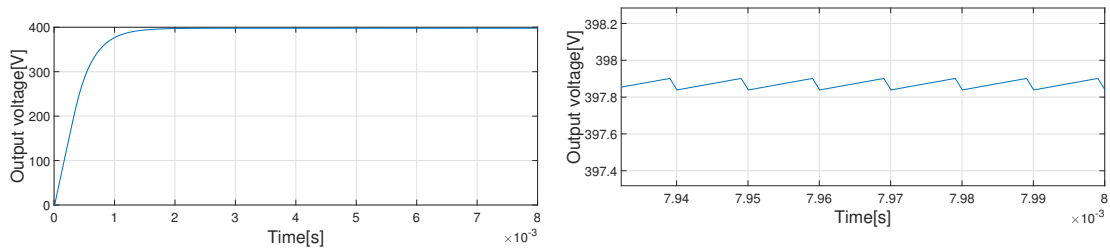


**Figure 4.9:** Output voltage for 2 converters

**Figure 4.10:** Output voltage ripple for 2 converters

The output voltage with a duty cycle of 0.45 gives 397.3V with 60mV.

#### 4.1.1.5 Cost analysis

The input current is calculated by using the datasheet from the fuel cell supplier. In Figure 3.1, the fuel cell voltage and the current characteristics is calculated from the datasheet.

A maximum input voltage is 165V which implies that each pair of MOSFETs should be able to handle a total voltage of 165V. For safety, the maximum drain to source voltage is taken as 165-200V per MOSFET.

Also, the maximum input current is 500A per MOSFET which is another constraint for the selection. With the parallel MOSFET connection, the current requirement is halved

i.e., 250A per MOSFET leg. However, the number of MOSFET legs are kept to be two to have a simple control, but still the efficiency comparison of the multiple MOSFET connection is listed in Table 4.4.

In case of the diode selection on the output side, the voltage limit should be higher than 378V considering the maximum DC link voltage of 378V. The maximum output current flowing through the diodes is 57A per converter at an input voltage of 90V and output voltage of 252V with two converters in parallel.

Market search based on the requirements suggested a few candidates and they are listed in Table 4.12. The online electronic distributors are Mouser, Digikey and Farnell. The cost of the core from Hitachi metals was not available without the quote. Thus the cost was found by using the smaller core with the same material and divided by the weight to find the per kg cost.

The required value in the table literally means required ratings for the components, and the market value means component ratings available on the market.

**Table 4.12:** Cost per 50000 DC/DC units for two isolated full bridge converters in parallel

Component (amount per unit)	Part number	Manufacturer	Required values	Market values	Cost [Units]
Transformer core-A (2)	T60004-L2160-W758	vacuumschmelze			1780.8million
Transformer wire-A (2)	CUL 100/0.1	BLOCK	38AWG	38AWG	284 million
Transformer core-B (2)	T60102-L2198-W160	vacuumschmelze			3032 million
Transformer wire-B (2)	CUL 100/0.1	BLOCK	38AWG	38AWG	227.2 million
Input filter capacitor(ceramic)	B58033I5206M001	TDK	17A, 17.7uF	58Apeak ,20uF	103.2 million
Output filter capacitor(electrolytic)(2)	ALA7DA681DF450	KEMET	25A, 202uF	3.06A, 680uF	22.4 million
Output filter capacitor(Ceramic)(23)	KTD501B105M76A0T00	United Chemi ON	25A, 202uF	1.08A ,1uF	48 million
Controllers and circuits	TMS320F28335PGFA	Texas Instrument			7267.5
MOSFET-A (8)	IXFK300N20X3	IXYS	165V, 250A	200V, 300A	222.4 million
Filter inductor (3)	PM2225NL	pulse engineering	114A, 5uH	130A, 2.1uH	10 million
Diode-A (8)	IDW75E60FKSA1	infineon	378V, 57A	600V, 120A	36 million
Diode-B (8)	VS-80EBU04	Vishay	378V, 57A	400V, 80A	42 million
Diode-C (8)	STTH100W04CW	STM	378V, 57A	400V, 100A	50.4 million
Heat sink(2)	122260	Wakefield - vette	0.644K/W	0.62K/W	181 million

The total cost for 50000 DCDC units varies from 3142 million units to 4466.32 million units in Table 4.12 depending on which diodes and transformers are chosen. Thus per unit the cost varies from 55520 to 89326.4 units.

The combinations of the components are two transformers and three diodes. Only when the cost is considered, (Diode-A, Transformer-A) is the best choice, which gives 13880 SEK per unit. However, Diode-A shows the highest voltage and current market values, meaning the loss might be highest among three. Thus, the efficiency calculation is iterated and shown in Table 4.13. The efficiencies are calculated based on the parameters at a junction temperature of 25°C.

**Table 4.13:** Loss values for component combinations

Loss [W] /(Diode,Tr)	A,B	B,B	C,B	A,A	B,A	C,A
<b>Input power</b>	45000	45000	45000	45000	45000	45000
<b>Total filter loss</b>	4.3	4.3	4.3	4.3	4.3	4.3
<b>Total MOSFET loss</b>	2258.7	2258.7	2258.7	2072.2	2072.2	2072.2
<b>Total diode loss</b>	410.3	266.71	358.95	433.89	282.05	379.6
<b>Total transformer loss</b>	163.29	163.29	163.29	104.34	104.34	104.34
<b>Efficiency</b>	93.6	93.9	93.71	93.55	93.89	93.67
<b>Total Cost [million units]</b>	4078.4	4099.8	4093.2	2776	2797.2	2790.8
<b>Per unit Cost [units]</b>	81568	81996	81864	55520	55944	55816

It is noticed that (B,A) and (B,B) shows the highest efficiency while (A,A) and (A,B) shows the lowest efficiency. However, the efficiency difference between them is only 0.4%, meaning that 180W of power is saved when at most 1302.4 million units per 50000 DC/DC units is spent more. The per unit cost in that case differs by 26048 units, meaning that 142% of (A,A) cost is equal to (B,B) cost with 0.3% of efficiency gain.

Thus, it is concluded that (Diode-A,Transformer-A) is a good option for two full bridge converters in parallel when the efficiency and the cost are considered. This result is subjected to change when the volume is considered.

The efficiency over output powers at different input voltages with selected components, (A,A) are shown in Figure 4.11.

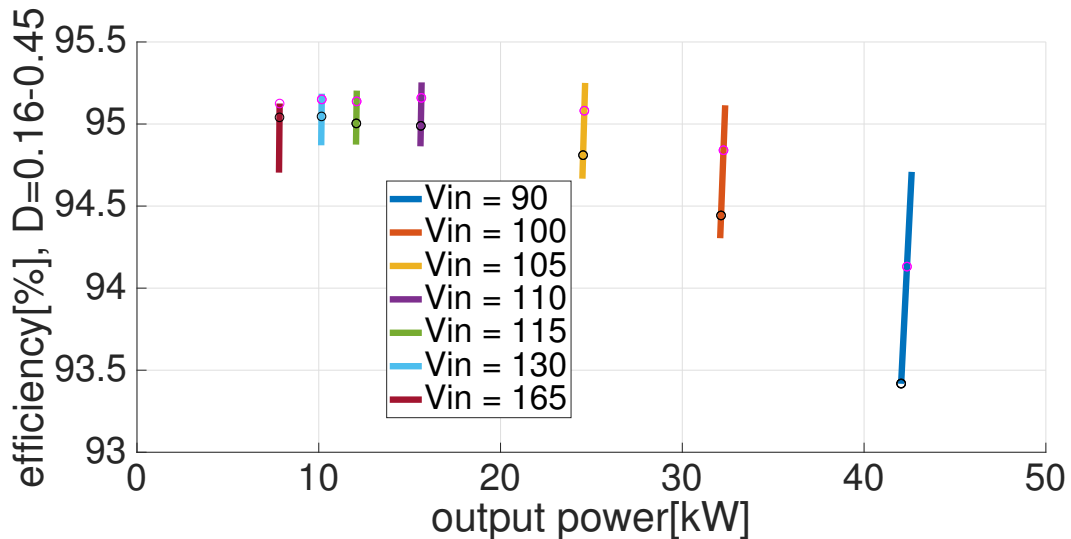


**Figure 4.11:** output power and efficiency with 2 legs, 2 converters in parallel with (A,A)

As compared with Figure 4.4, it is seen that the efficiency is increased by 6.5% at highest and 2% at lowest.

#### 4.1.1.6 Dual active bridge cost analysis

The diodes in the full bridge converters are replaced by MOSFETs for several purposes: soft switching and bidirection of power flow. In this thesis, unidirection is used to ensure that no current flows from the battery or the inverter to the fuel cell stack. However, due to reasons stated in 3.2.1, the dual active bridge topology is considered when comparing cost.

The MOSFET chosen is IXFB132N50P3, with a reverse break down voltage of 500V, drain current at 25° C of 132A while the required value is the same for the diodes in Table 4.12.

The cost for the parallel converters with MOSFETs on the output side is 158.096 million units, meaning that the per unit cost of MOSFETs on the output side is 3161.92 units extra. The overall cost when the transformer A is used, is 3265.2 million units, increased by 30.7 million units as compared to (A,A) case in Table 4.11. Thus using the values from Table 4.13, the DC/DC cost per unit comes out to be 65304 units.

#### 4.1.1.7 Volume Analysis

The volumes for each component in the isolated full bridge converter, two in parallel are listed in Table 4.14.

**Table 4.14:** Volume for components in two isolated full bridge converters in parallel

components (amount per unit)	length[cm]	width[cm]	height[cm]	total [cm <sup>3</sup> ]
Transformer A (2)	16	16	2.5	776.8
Transformer B (2)	19.8	11.5	3.1	1353
Input capacitors (1)	2.2	3.3	1.15	8.349
Output capacitor-electrolyte (2)	5	3.5	1	35
Output capacitor-ceramic (23)	1	1	0.38	8.74
Filter inductor (3)	6	4.75	2.85	81.225
MOSFET (8)	1.61	0.52	4.19	28.056
Diode-A (8)	1.61	0.521	4.14	27.728
Diode-B (8)	1.95	0.495	3.98	30.72
Diode-C (8)	1.58	0.515	3.5	22.72
Heatsink (2)	30	7.5	23	10350

The volumes for all combinations of the components (Diode,Transformer) in the isolated full bridge converter, two in parallel are listed in Table 4.15. The total volume is calculated by using the power density of the converters with a similar topology available in the market.

#### 4. Analysis

**Table 4.15:** Volume results for two isolated full bridge converters in parallel

combination	total component volume[ $cm^3 / L$ ]
<b>A,B</b>	11890 / 11.89
<b>B,B</b>	11895 / 11.90
<b>C,B</b>	11887 / 11.89
<b>A,A</b>	11314 / 11.31
<b>B,A</b>	11319 / 11.32
<b>C,A</b>	11311 / 11.31

In Table 4.15, only component volumes are calculated by adding up all volumes in Table 4.14 both in  $cm^3$  and  $L$ . It results that the diodes do not affect to the total volume much while the transformer affects more. Thus volume wise, having transformer-A is a good option.

The actual volume, the component volume and the air volume added together, is estimated by using the design reference from DC/DC converters used for a similar kind of applications. A 54kW isolated DC/DC converter from TAME POWER has a total volume of 30.225  $L$ . Thus the power density is 1.7kW/ $L$ . Also the conventional isolated DC/DC of 2.5kW has a power density of 1.6 kW/ $L$ . This suggests a margin for the design of 45 kW Full bridge Isolated converter.

Using the 54kW converter from TAME POWER which has the power density for minimum volume, the total volume for the 45kW converter is calculated to be 26.47L.

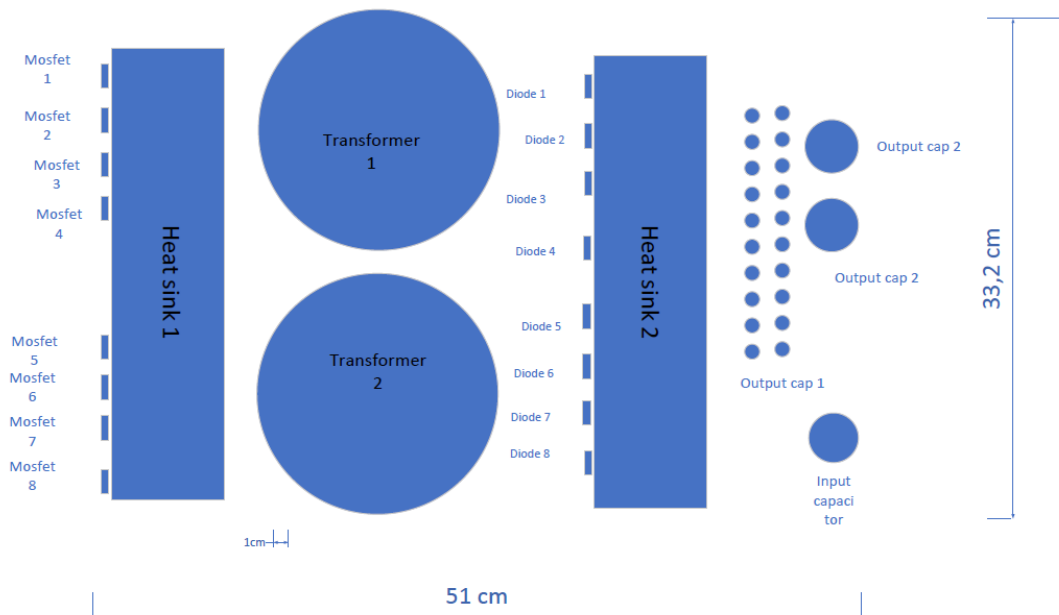


**Figure 4.12:** Components arrangement for the isolated converter

Figure 4.12 shows the arrangement of the components for the isolated boost converter. Considering the minimum spacing of  $1\text{cm}$  between the components [20] and placing the transformers in such a way that only enough space is left void, the total length comprises of the transformer lengths and the minimum spacing between them and this value is calculated as  $33.2\text{ cm}$ . The rest of all the components are placed width wise and the total value is  $51\text{ cm}$ . Also considering the heat sink design calculations, the height of the DC/DC can be approximated as the height of the heat sink and the control board on the top, i.e.,  $24\text{cm}$ . So the total volume is calculated as  $38.9\text{ L}$ .

The 3D modelling for the isolated converter was done by using Catia V5 for clear understanding of the volume analysis and is shown in Figure 4.13.

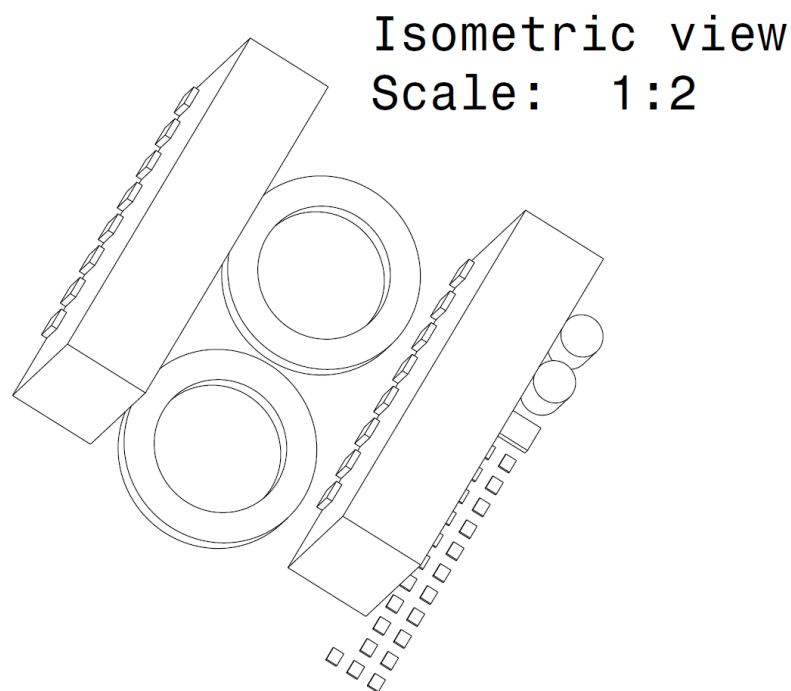


**Figure 4.13:** 3D model for the isolated converter-isometric view

The windings in the cores are neglected in the drawing. To compensate the space for windings, the space between cores are increased by twice, having  $20\text{mm}$  of spacing in between. Also, it is placed in order to occupy the lesser space. This means the input capacitor and the output electrolyte capacitors shown in Figure 4.12 is moved next to output ceramic capacitors. Therefore, according to Figure 4.13, the total volume is shown in Figure 4.14.

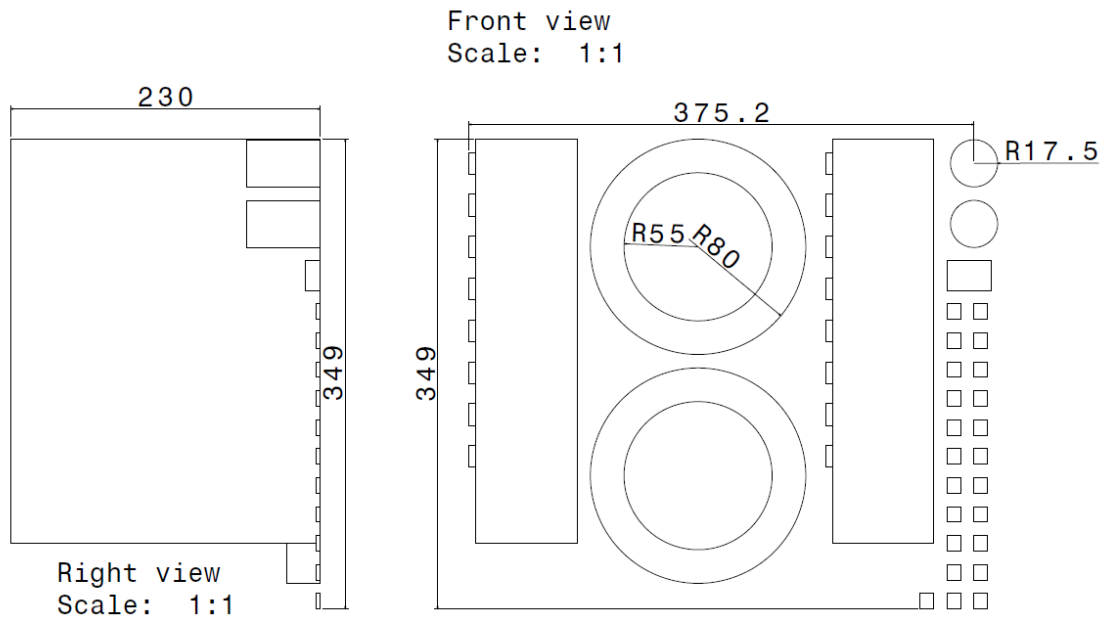


**Figure 4.14:** 3D model for the isolated converter-front and right view

It is shown in Figure 4.14 that total length is  $392.7\text{mm}$ , total width  $349\text{mm}$  and total height  $230\text{mm}$ . This results in total of  $31.52\text{L}$ .

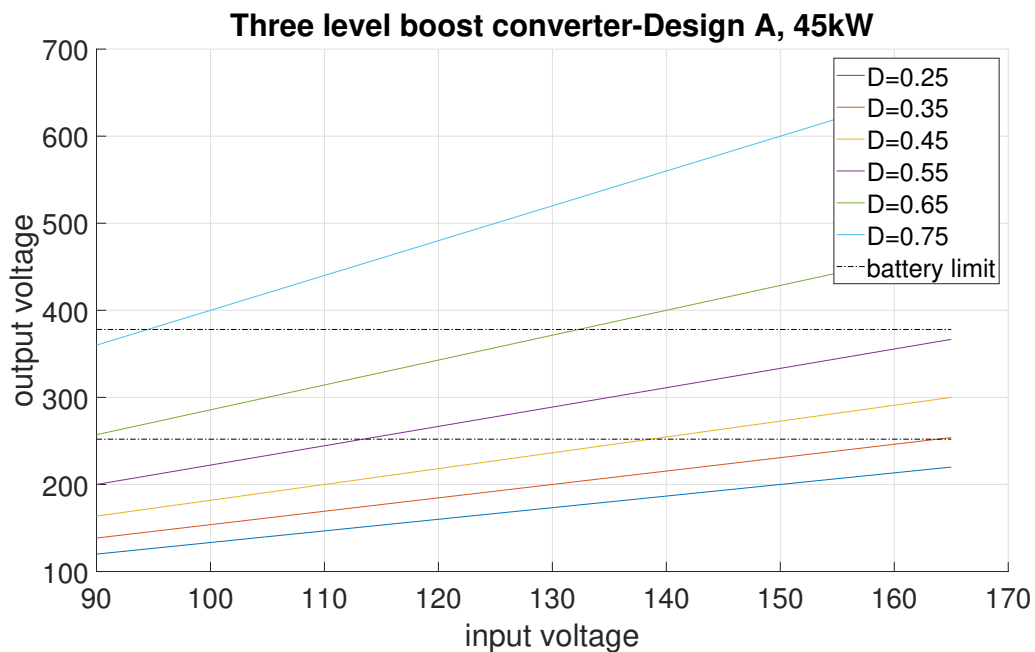
This value is not close to the one calculated using power density calculations as it is a very rough estimation. A PCB design would give much better estimation of the volume.

## 4.1.2 Non-isolated three-level boost converter

This section is about the design, voltage and current waveforms of a three-level boost converter. The efficiency of the converter will be put forth and simulation of it will be shown.

### 4.1.2.1 Control Strategy

This section has a focus on the control of the converter with respect to the Duty cycle. The graph generated as shown in Figure 4.24 is generated in MATLAB by calculating the output voltage for an input voltage range of  $90\text{V}$ - $165\text{V}$  using (2.22).



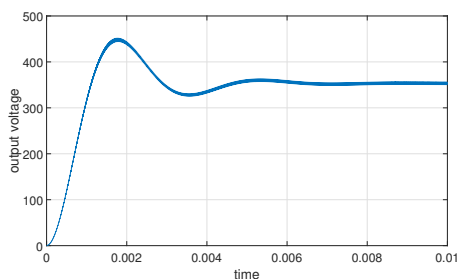
**Figure 4.15:** Duty cycle variation for the voltage profile

Figure 4.24 shows the duty cycle variation for different input and output voltages. The dotted line represents the maximum output voltage required (378V). At an input voltage of 90V and a duty cycle of 0.25, the output voltage is 110V while for 0.75 it is 378V. For a nominal voltage of 130V, the maximum voltage is attainable at the duty cycle 0.65. At the maximum input voltage 165V, the output is 378V at  $D=0.55$ .

#### 4.1.2.2 Simulation

In Figure 2.7, a model of a three-level boost converter is shown.

The input voltage is 90V and the duty cycle is the maximum duty cycle calculated by (2.23) and the load resistor is calculated by (3.1). Inductors and capacitors are selected by (2.24) and (2.14). The low side switch has a 180 degree of delay.



**Figure 4.16:** Output voltage- three level boost converter

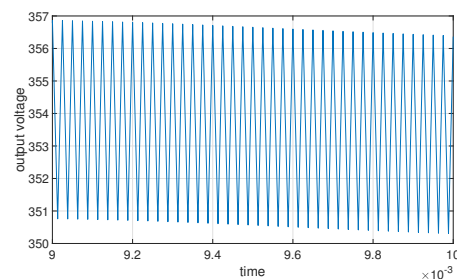


**Figure 4.17:** Output voltage ripple- three level boost converter

It is shown that the output voltage is 354V in Figure 4.16 with 6V of the peak to peak ripple in Figure 4.17.

## 4. Analysis

---

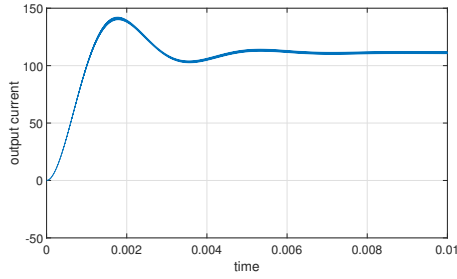


**Figure 4.18:** Output current- three level boost converter

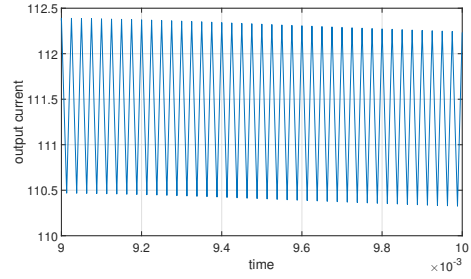


**Figure 4.19:** Output current ripple- three level boost converter

It is shown that the output current is 111.5A in Figure 4.18 with 2A of the peak to peak ripple in Figure 4.19.

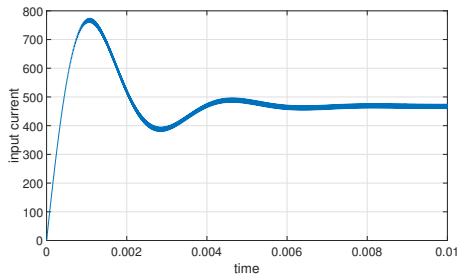


**Figure 4.20:** Input current- three level boost converter

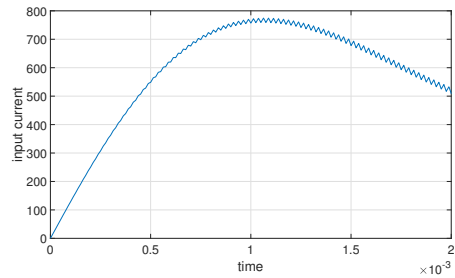


**Figure 4.21:** Input peak current- three level boost converter

It is shown that average input current is 467A in steady state in Figure 4.20 with 775A of peak in Figure 4.21.

As can be seen in Figure 2.7, it has more components than normal boost converters, meaning it is complicated. Also, due to its rare usage, it is determined to compare a three-phase boost converter, which is three normal boost converters connected in parallel with phase shift.

### 4.1.3 Non-isolated three-phase boost converter

A three phase boost converter is evaluated below in this section. Here the design, voltage and current waveforms are shown. Also efficiency, cost and volume analysis are done.

#### 4.1.3.1 Loss calculation

This section is about the loss calculation and efficiency comparison of non-isolated converter for the different number of phases. However the main analysis is done only for the three phase as shown in Figure 4.24, Figure 4.22 and Figure 4.23. The loss calculation

for the components in converters with different number of phases is shown in table 4.17.

In Table 4.16, the parameters used for loss calculation are specified.

**Table 4.16:** Parameters for a three phase boost converter

	values
switching frequency [kHz]	50
ripple current [A]	33.4, i.e., 20% of $\frac{500}{3}$ A
inductance [uH]	56
ripple voltage [V]	9, i.e., 10% of 90
capacitance [uF]	198

**Table 4.17:** Loss values for converters with different phases

Type of loss[W]/number of phases	1	2	3	4
input power	45000	45000	45000	45000
MOSFET conduction per unit	907.35	226.84	100.82	56.71
MOSFET switching per unit	348.75	174.38	116.25	87.188
MOSFET dead time per unit	60.45	30.225	20.15	15.113
total MOSFET loss	1316.7	863.27	712.25	636.84
diode conduction per unit	43.557	21.78	14.52	10.89
diode switching per unit	0.0025	0.0025	0.0025	0.0025
diode off time per unit	60.73	60.73	60.73	60.73
total diode loss	104.28	165	225.7	286.45
total copper loss	103.2	83.93	26.3	7
total core loss	17.64	35.28	59.7	56
total filter loss	1.52	1.52	1.52	1.52
efficiency[%]	96	97.75	98.47	98.67

Table 4.17 shows that the efficiency increases with the number of phases used. However the difference in the efficiency between the three-phase and the four-phase is less than 0.02 % while a three-phase boost converter gives 98.47 % efficiency. Hence a three phase is a good option in this application. Moreover going for more phases with increased components only for 0.02 % efficiency is not a good trade-off.

Also the complexity of control is reduced with one less phase. With lesser phases the losses are high and the components for their ratings are difficult to find in the market.

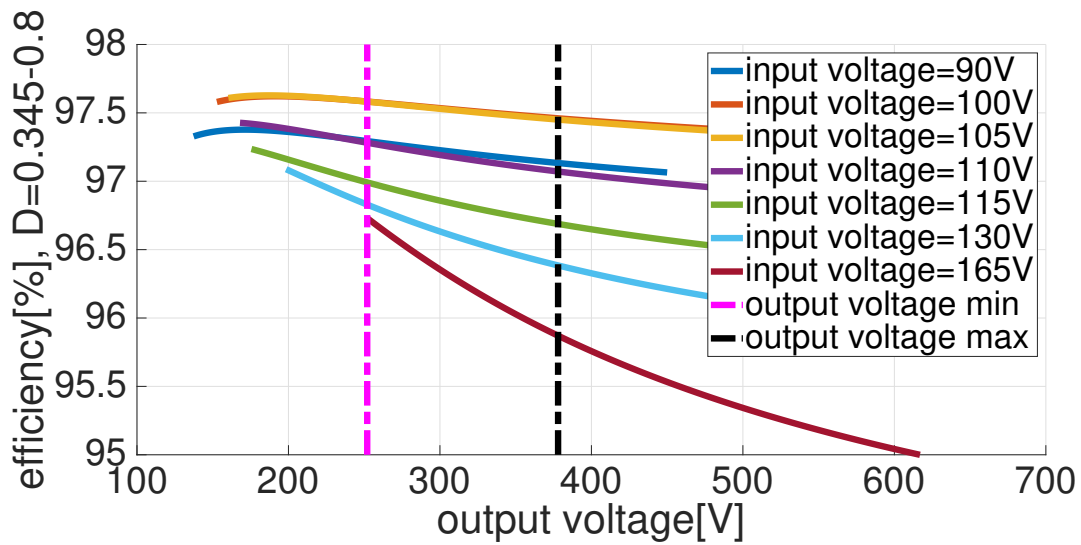


**Figure 4.22:** output voltage over efficiency for the three-phase boost converter

Figure 4.22 shows that the efficiency range as function of the output voltage range (252V - 378 V) represented by the pink and black dotted line respectively at different input voltage levels. The efficiency gradually decreases from 97% to 96.3% at an input voltage of 165V. The efficiency is highest at an input voltage of 100V and it varies from 97.9% to 97.8% for the required output range.

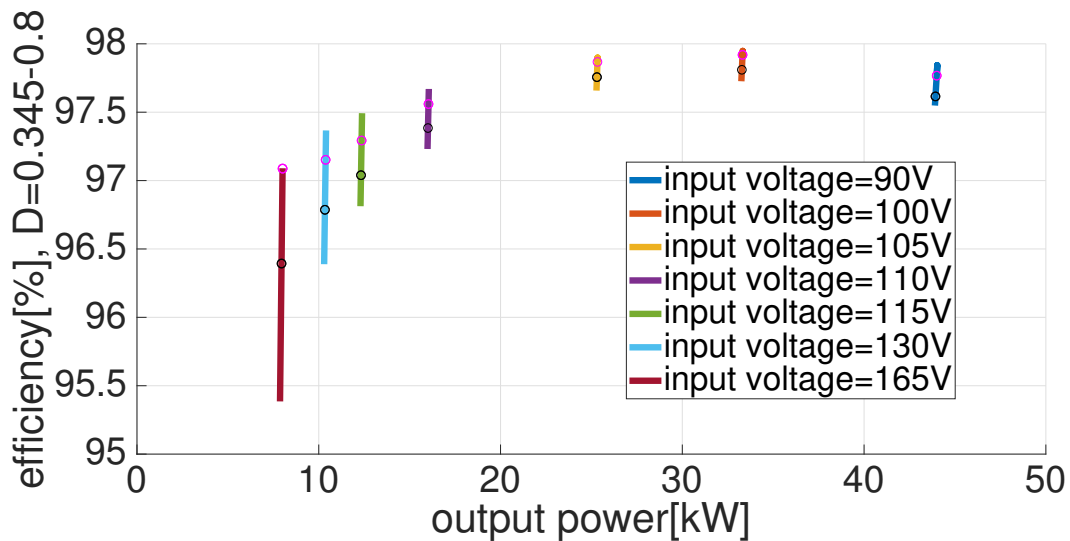
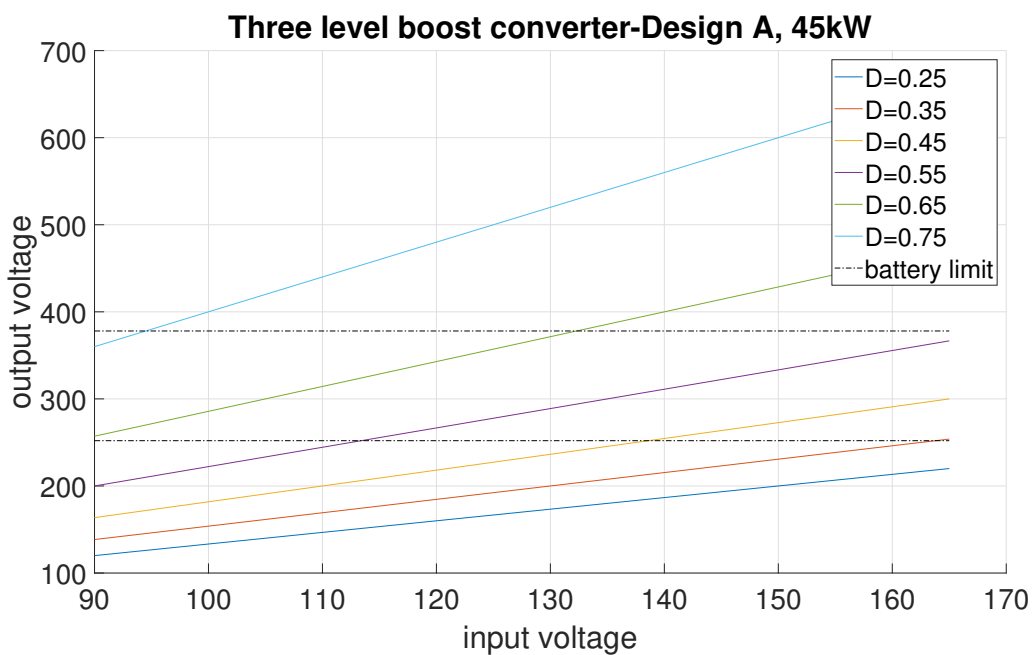


**Figure 4.23:** output power over efficiency for the three-phase boost converter

Figure 4.23 illustrates the efficiencies for different operating power levels of the converter. For an input voltage of 90V from the fuel cell, the input current is 500A which gives a maximum output power close to 45kW. However, as different from what is explained above in the isolated boost converter, the highest current does not lead to the highest losses and hence a lower efficiency. Rather, at the highest input voltage and the lowest input current with the maximum duty cycle for that input voltage, it shows the lowest efficiency. The reason here is that the proportion of the core loss, which is always constant

regardless of input and output voltage is higher at minimum output power. As the duty cycle increases, the output voltage increases whereas output current decreases. Thus, at lower output voltage, the power losses in diodes increases, leading to lower efficiency.

#### 4.1.3.2 Control strategy



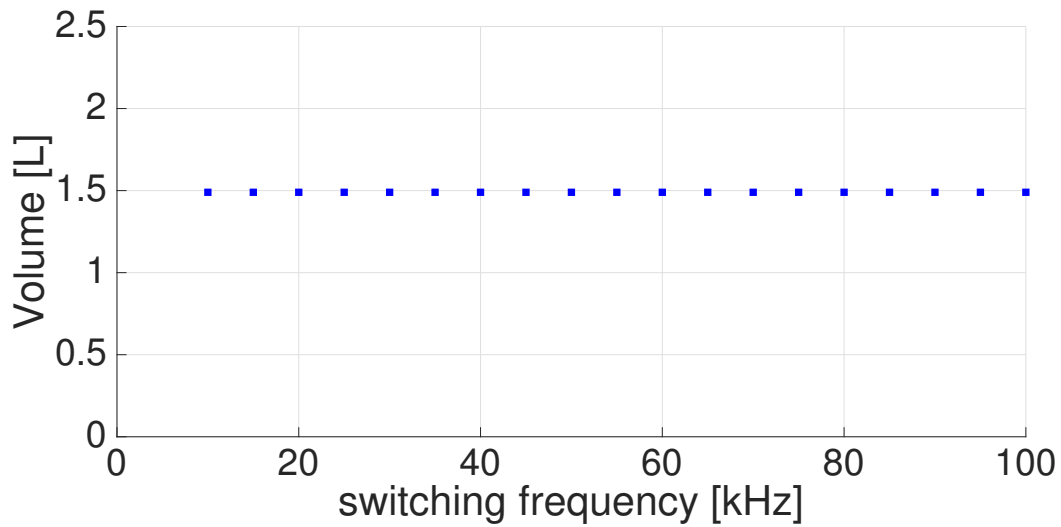
**Figure 4.24:** Duty cycle variation for the voltage profile

Figure 4.24 shows the duty cycle operation range within the battery limit. For 90 V input, maximum DC link voltage of 378 V can be obtained at the duty cycle of 0.75 while for 165V input, the duty cycle required is 0.55 for the same output voltage.

#### 4.1.3.3 Inductor and wire setup

Figure 4.25 shows the required inductor volume as a function of switching frequency with the same ripple current and ripple voltage as in Table 4.16. This figure is used to see if the used switching frequency of 20kHz results in which volumes of inductors, since inductance value is calculated by (2.24), which depends on switching frequency  $f_{sw}$ .

The core for an inductor is FINEMET® F3CC Series Cut Core from Hitachi Metals [11] and the values are listed in 2.1 as a core C. The changed inductance and capacitance parameters for a three-phase boost converter is specified in Table 4.18.



**Figure 4.25:** inductor volume over frequency with core area in Table 2.1

Figure 4.25 shows that higher switching frequency results in a lower volume of inductors according to (2.26). The volume for the boost inductors and the wires remains the same volume. Thus, volume-wise it is decided that 50kHz, the same switching frequency as the isolated full-bridge converter, will be used for simulation and cost analysis.

In Figure 4.26, the air gap length  $l_g$  in blue color, at 50kHz calculated by (2.54) is 0.35 cm with the number of turns being 15. It is noticed that the air gap length  $l_g$  is sufficient for the core not to saturate. The peak flux density without the fringing flux in red color  $B_{peak}$  is calculated with (2.58). The saturation flux for this core is 1.23T as can be found in Table 2.1.

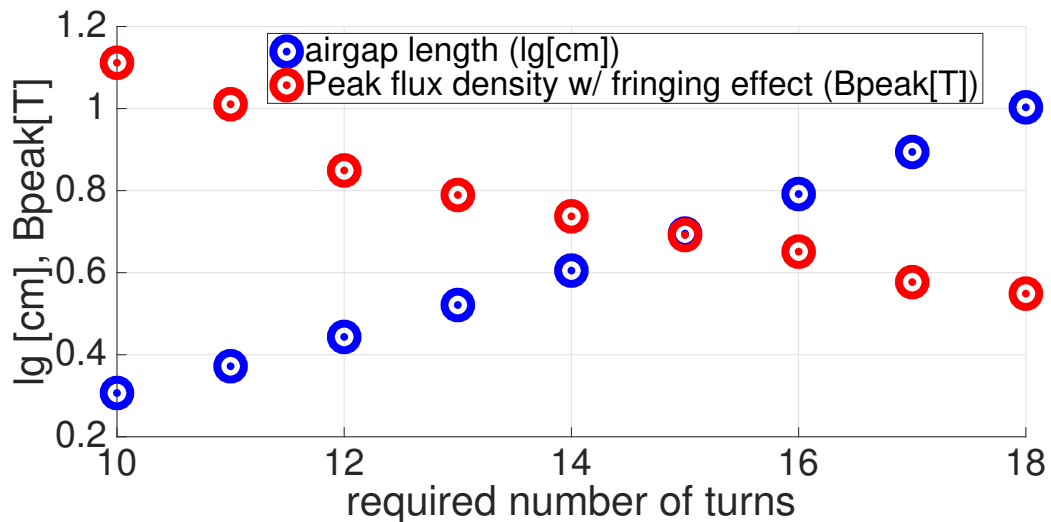


**Figure 4.26:** air gap length and flux density over the number of turns

However, the peak flux density in green color in the same figure shows a lower peak value since the fringing flux effect calculated by (2.55) is considered. Thus, the new number of

turns calculated with (2.56) is 14.

The original core from Hitachi Metals does not have air gap [11]. However, an air gap is introduced to reduce the inductance and increase the current at the core saturation point since the low inductance value (55.8uH) with the highest current (184A) is required as can be seen in Table 4.18.

The fringing flux is caused by introducing the air gap and is assumed to be zero when calculating the air gap length since the fringing flux depends on different factors [19].

However, assuming that the fringing flux is zero affects the volume of the inductor since the longer the air gap is, the more the fringing flux becomes and thus the peak flux density is decreased. This affects the fringing flux factor  $F$ , as can be seen in (2.55) and the new number of turns, as can be seen in 2.56. Since the real window utilization factor is affected by the core material, wire lay and wire insulation type and the number of turns [10], the fringing flux should not be assumed to be zero in an accurate calculation.

All the calculation in this section is done with parameters in Table 4.18.

**Table 4.18:** Parameters for a three phase boost converter

	values
<b>switching frequency [kHz]</b>	50
<b>ripple current [A]</b>	34, i.e., 20% of $\frac{500}{3}$ A
<b>inductance [uH]</b>	55.8
<b>ripple voltage [V]</b>	9, i.e., 10% of 90V
<b>capacitance [uF]</b>	191.5

With the parameters in Table 4.18, the efficiency does not change much according to Table 4.19. The efficiency is calculated in the worst case scenario: minimum input voltage and maximum output voltage.

**Table 4.19:** Loss values of a three phase boost converter for different frequencies

	20kHz	50kHz	80kHz	100kHz
<b>efficiency [%]</b>	97.35	97.18	96.67	96.32

At 20kHz, the efficiency is 97.35% whereas the efficiency at 50kHz is 97.18%. The difference between those efficiencies is only 0.7%. However, at 80kHz, the efficiency decreased by 1.5% as compared with 50kHz. Thus, using 50kHz in the nonisolated boost converter is proved to be a good assumption in efficiency-wise.

In Table 4.20, the result parameters for the three-phase boost inductors per unit.

**Table 4.20:** Results for wire and core setup for boost inductors per unit

Wire	values
length [m]	2.7
number of wires per bundle	5556
number of turns with airgap	13
wire mass [kg]	1.17
winding resistance [mohm]	0.08
copper loss [W]	7.14
Core	values
required inductance [uH]	55.8
obtained inductance [uH]	58.4
airgap length [cm]	0.34
required window utilization factor	0.37
obtained window utilization factor	0.33
core mass [kg]	2.84
core loss [W]	20
temperature rise [°C]	117.2

The wire length for the number of turns 13 is 2.7m when winding layers by (2.33) and (2.34) are considered. The wire mass is calculated by (2.36) with  $\rho_{v.wire}$  of  $11130 \text{ kg/m}^3$ . Winding resistance is calculated by (2.46) with  $\rho_{wire}$  of  $17.122 \text{ ohm-cm}$ , which is calculated from resistance of wire per meter multiplied by area of the wire. The copper loss is calculated by (2.50) and  $\Delta i_L$  can be seen in Table 4.18.

The obtained inductance,  $58.4\mu\text{H}$  is calculated by (2.57) which is 5% higher than the required value of  $55.8\mu\text{H}$ . The window utilization factor is obtained to be 0.23 by using (2.42) with only having  $k=1$ , while the required window utilization factor is 0.37 calculated by (2.41). Thus the core size can be reduced further with the similar surface area and with the smaller window area.

#### 4.1.3.4 Simulation

The model used for simulation of the three-phase boost converter is shown below in figure 4.27.

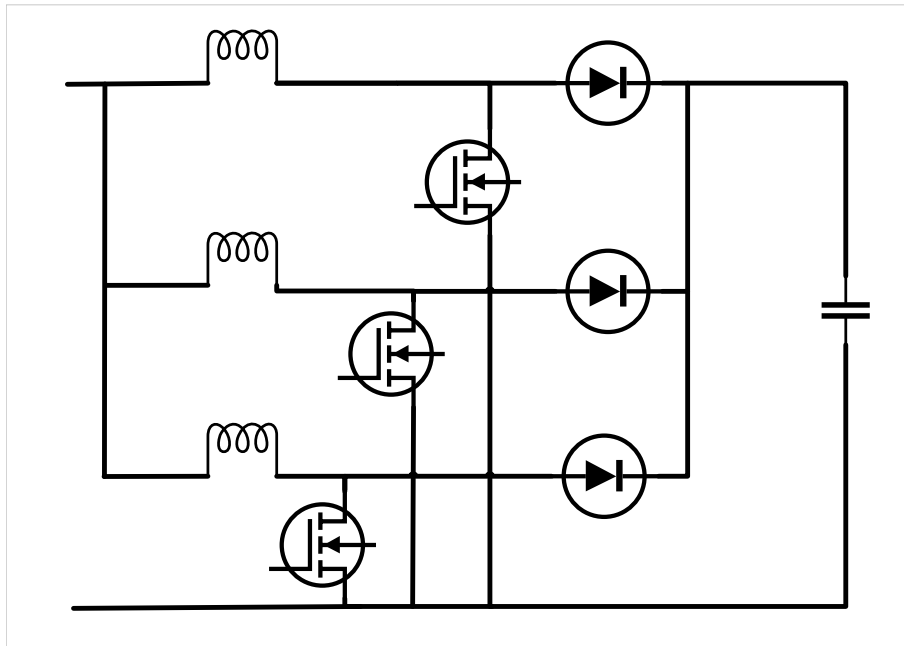


**Figure 4.27:** Three phase boost converter

The input voltage is 90V and the duty cycle is the maximum duty cycle calculated by (2.23) i.e 0.76 and the load resistor is calculated by (3.1). Inductors and capacitors are selected using (2.24) and (2.14).

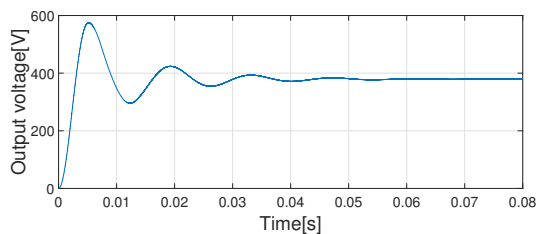


**Figure 4.28:** Output voltage for boost

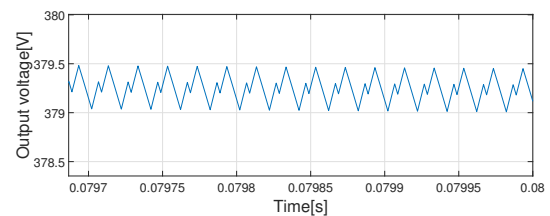


**Figure 4.29:** current ripple for boost

Figure 4.28 shows that the average output voltage is 373 V which is the expected value and Figure 4.29 shows a ripple value of 1V peak to peak.

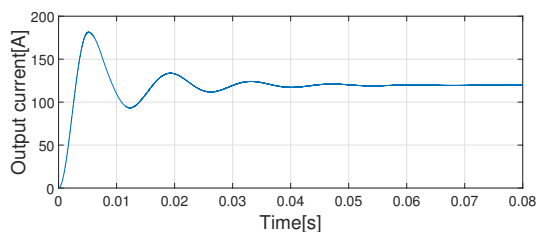


**Figure 4.30:** Output current for boost

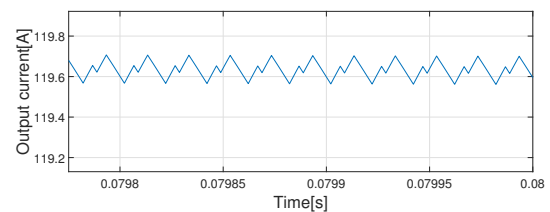


**Figure 4.31:** current ripple for boost

Figure 4.30 shows the average output current to be 119.5 A and 4.31 shows the ripple value of 18mA peak to peak.

### 4.1.3.5 Cost analysis

Since it is a three-phase boost converter, the input current of a maximum value 500 A is split into 3 paths and hence the current requirement for the inductor is decreased. For the inductor design, Core C in Table 2.1 with an inductance of 58.4 $\mu$ H as shown in Table 4.18 is used. The air gap is used to reduce the inductance and increase saturation point, and has a value of 0.42 cm. The per kg cost is 4479.2 units. The inductor wire is CUL 100/0.1 and per kg cost is 4139.2 units.

The peak to peak ripple current is 34A per phase and 11.4A with the phase shift. However, the maximum peak to peak current calculated by (2.49), where  $V_{in} = 165$ ,  $D = 0.56$ ,  $L = 65.12\mu H$ , is 28A. Thus, when the current ripple is considered, 23 pieces of ceramic capacitor KTD501B105M76A0T00 each with a max ripple current of 1.05A were placed in parallel at the output. Also at the output, 2 quantities of aluminum electrolytic capacitor ALA7DA681DF450 with a max ripple current of 6.49A (at 100kHz) are connected in series with a value of 680 $\mu$ F and 400V each. They are used for their high ripple current handling capacity and for energy transfer.

Also 3 quantities of the diode VS-150EBU04 each with a reverse breakdown voltage capacity of 400V and an average current of 150 A, maximum 300A with 20kHz per phase were chosen when the output voltage is 378V and the maximum efficiency is 98.7%. The maximum current flowing through a MOSFET is 167A with current ripples, 20% of input current. 3 quantities of MOSFET IXFB210N20P, each with a maximum drain to source breakdown voltage of 200V and current of 210A considering a safety margin of 10 percent. The material of this MOSFET is Silicon.

The input capacitor value is calculated by using (2.13) and is equal to 13.3 $\mu$ F. The capacitor value available closest to this in the market is B58033I5206M001 and has specifications of 20 $\mu$ F and 500V of voltage ratings. The ripple capacity of this capacitor is 41A rms.

For the heat sink with forced air cooling, the thermal resistance of sink to ambient  $R_{thsa}$  was calculated using (2.17), where the  $R_{thjc}$  and  $R_{thcs}$  values are available from the MOSFET and the diode data sheets. Also the ambient temperature is 85°C. F is calculated as 0.23 using the maximum air flow (D) of 350  $m^3/hr$  [22]. Thus  $R_{thsa}$  is 0.664 and the heat sink closest to this value in the market is 0.62K/W from Wakefield-vette.

All the components with part names, manufacturers and costs are listed in Table 4.21.

**Table 4.21:** Cost analysis for a 3phase boost converter

Component	Part name	Manufacturer	Required Value	Market Value	Cost for 50 000 DCDC converters(units)
Inductor core	F1AH1266	Hitachi metals	56uH	58uH	1909.52 million
Inductor wire	CUL 100/0.1	BLOCK			50.4 million
Input filter capacitor(ceramic)(1)	B58033I5206M001	TDK	13.3uF	20 uF, 500V	104 million
Output filter capacitor(electrolytic)(2)	ALA7DA681DF450	KEMET	191uF	680uF, 6.5A (10kHz)	22.4 million
Output filter capacitor(Ceramic)(23)	KTD501B105M76A0T00	United Chemi ON	198uF	1uF, 1.05A	44.8 million
Mosfet(3)	IXFB210N20P	IXYS	165V, 167A	200 V, 210 A	86.4 million
Diode(3)	VS-150EBU04	Vishay	378V, 167A	400V, 150A	24.8 million
Heat sink(1)	122260	Wakefield - vette	0.644K/W	0.62K/W	91.2 million
Controllers and circuits	TMS320F28335PGFA	Texas Instrument			29070
			<b>Total Cost =</b>		2333.52 million units
			<b>Cost per unit=</b>		46670.4 units

The cost analysis as seen from Table 4.21 was done for 50,000 DCDC units including the estimated cost of the PWM controller and the driver circuit and then finally the cost per DCDC unit was calculated as an average.

**Table 4.22:** Cost analysis for a 4phase boost converter

Component	Product	Manufacturer	Required Value	Market Value	Cost for 50 000 DCDC units(units)
Inductor core	F1AH1266	Hitachi metals			2546 million
Inductor wire	CUL 100/0.1	BLOCK			49.6 million
Input filter capacitor(ceramic)(1)	B58033I5206M001	TDK	13.3uH, 165V	20 uF,500 V	103.2 million
Output filter capacitor(electrolytic)(2)	ALA7DA681DF450	KEMET	198uH, 378V	680 uF	22.4 million
Output filter capacitor(Ceramic)(23)	KTD501B105M76A0T00	United Chemi ON	191uH, 378V	1 uF	44.8 million
Mosfet(4)	IXFB210N20P	IXYS	165V, 150A	200 V, 210 A	115.6 million
Diode(4)	IDW75E60FKSA1	infiniton	378, 150A	400V, 120A	15.28 million
Heat sink(1)	122260	Wakefield - vette	0.644K/W	0.62K/W	91.2 million
Controllers and circuits	TMS320F28335PGFA	Texas Instrument			29070
			<b>Total Cost =</b>		2986.4 million
			<b>Cost per unit=</b>		57568 unit

The cost analysis for a four-phase boost converter is done as seen in Table 4.22. It shows that the cost per DC/DC unit is 59728 units. Thus a difference of 12800 units per converter as compared with a three-phase boost converter is observed. This is majorly because of the increased number of boost inductors in 4phase converter and the increased cost of the MOSFETs. The unavailability of MOSFET for a relative lower value of current for the same voltage of 200V makes it necessary to use the same MOSFET as in the three-phase boost case. The inductor design values for a value of 58.4 uH can be seen in Table 4.22 where the core and the wire values are higher than for the 3 phase inductors.

At the worst scenario, the efficiencies and losses change with the new components in Table 4.21 and Table 4.22, and the result is specified in Table 4.23.

**Table 4.23:** Loss values for boost converters

Loss [W]	(3 phase)	(4 phase)
<b>Input power</b>	45000	45000
<b>Total MOSFET loss</b>	629.55	503.62
<b>Total diode loss</b>	26.26	26.3
<b>Total inductor loss</b>	7.147	7.014
<b>Total core loss</b>	20	20
<b>Efficiency [%]</b>	98.477	98.774

The efficiency difference between a three-phase boost and a four-phase boost is only more 0.3%. 640 million units for 0.3% does not earn much. Thus, three phases are optimal

when both the cost and the efficiency are considered.

In Figure 4.32, the efficiency of the three-phase boost converter with the selected components is shown.

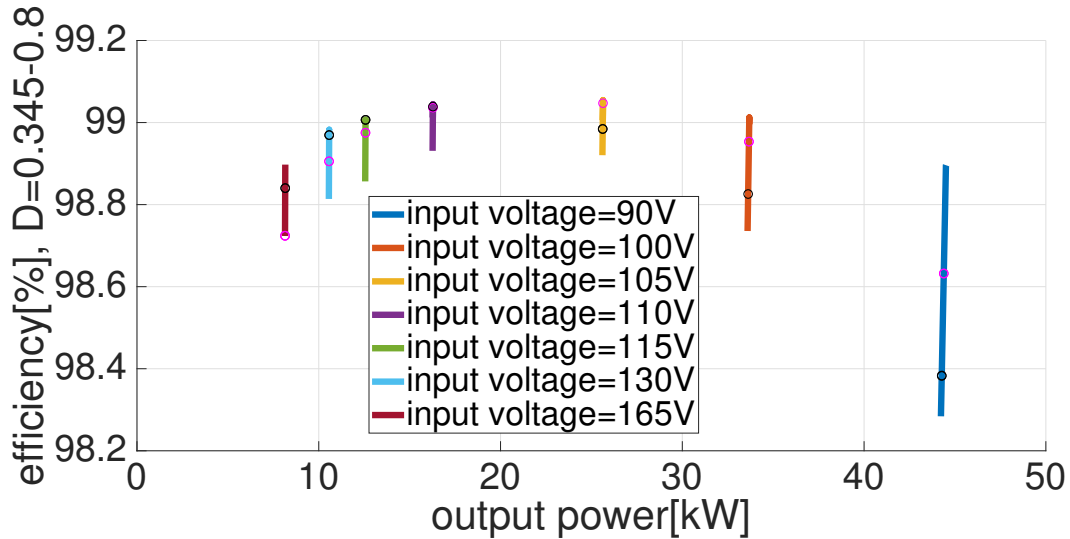


**Figure 4.32:** Efficiency over output power for the three-phase boost converter with selected component

It is seen that with the components with proper values, the maximum efficiency is increased by 1% compared with the maximum efficiency with the oversized components, 97.9% in Figure 4.23.

#### 4.1.3.6 Volume analysis

The volumes for each component in the three-phase boost converter are listed in the Table 4.24.

**Table 4.24:** Volume for each component in the three-phase boost converter

components	length[cm]	width[cm]	Thickness[cm]	amount	total volume[cm <sup>3</sup> ]
<b>Input capacitors</b>	2.2	3.3	1.15	1	8.349
<b>Output capacitor 1</b>	5	3.55	1	2	35.5
<b>Output capacitor 2</b>	1.15	1	0.38	23	10.051
<b>Boost inductor</b>	17.34	10.14	3.5	3	1846.19
<b>MOSFET</b>	2.659	2.029	0.531	3	8.594
<b>Diode</b>	3.98	1.22	0.3	3	4.37
<b>Heat sink</b>	30	7.5	23	1	5017.5

A 40kW non isolated DC/DC converter from TAME POWER i.e CONV-DCDC-40KW-GILS-01-K has a total volume of 20.6litres. Thus the power density is calculated as 0.0019kW/cm<sup>3</sup>. Also the conventional non isolated DCDC of 11kW from TDK i.e EZA11K320240 has a power density of 0.0011 kW/cm<sup>3</sup>. This suggests a margin for design of 45kW non isolated converter. Using the 40kW power density as a reference for minimum volume,

the total volume for the 45kW converter is calculated as 23.7 litres.

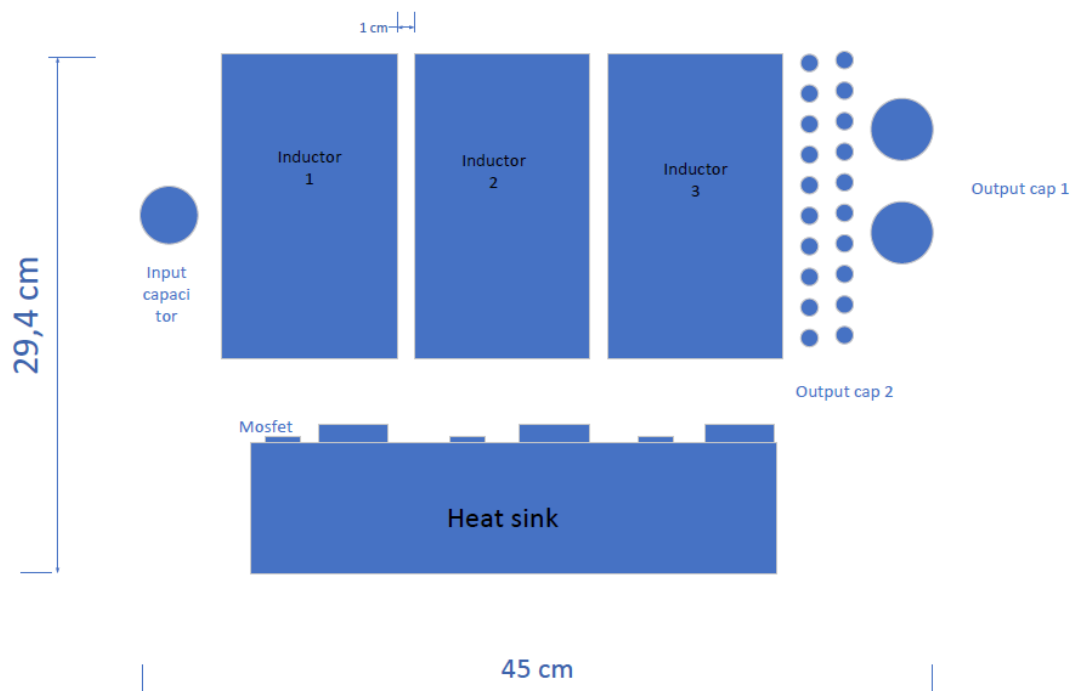


**Figure 4.33:** Components arrangement for the non isolated converter

From Table 4.24, it is observed that the maximum space is occupied by the boost inductor. Considering a minimum spacing of 1 cm between the components spacing rule and placing the inductors width wise in series gives a total value of approximately 42 cm. Since the inductor is placed width wise as seen in the Figure 4.33, the length of one inductor represents the length of all the inductors. So the other dimension of the converter equals the screwmounted MOSFET length, minimum spacing and the length of the boost inductor. The value is calculated as 29.5cm. The height of the DC-DC can be approximated as that of the heat sink i.e 23cm. Thus the total volume is 28.5 litres which is not so close to the one calculated using power density.

The 3D modelling for the non isolated converter was done by using Catia V5 for clear understanding of the volume analysis and is shown in Figure 4.34.

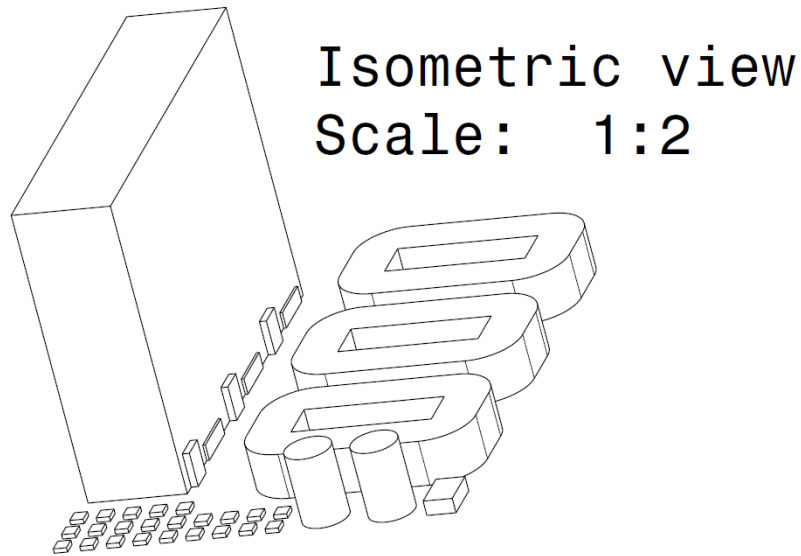


**Figure 4.34:** 3D model for the non isolated converter-isometric view

The airgaps in the cores and the windings are neglected in the drawing. To compensate the space for windings, the space between cores are increased by twice, having 20mm of spacing in between. Also, it is placed in order to occupy the lesser space. This means the input capacitor shown in Figure 4.33 is moved next to output capacitors. Therefore, according to Figure 4.34, the total volume is shown in Figure 4.35.

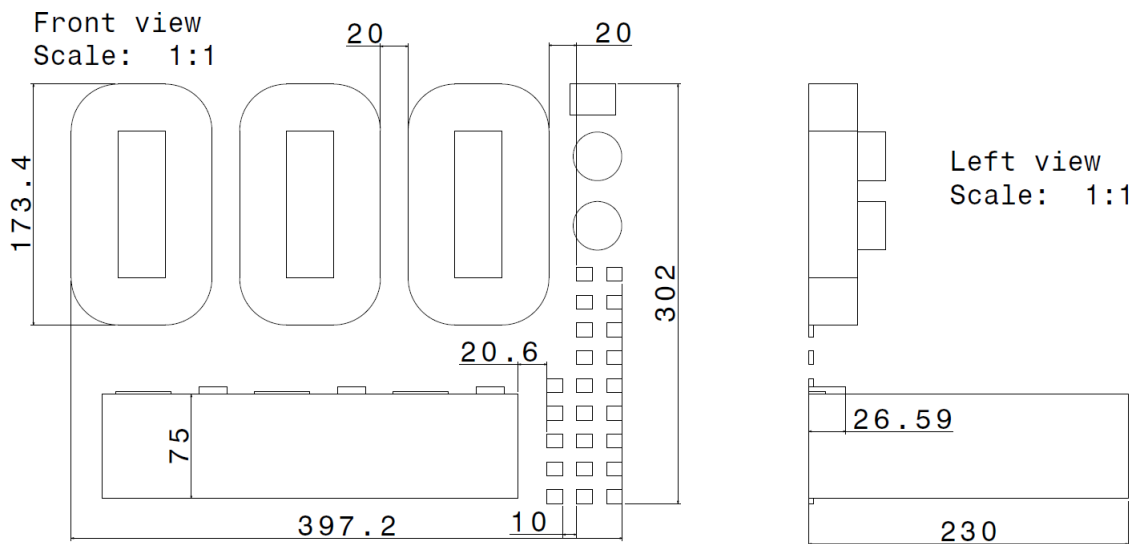


**Figure 4.35:** 3D model for the non isolated converter-front and left view

It is shown in Figure 4.35 that total length is 397.2mm, total width 302mm and total height 230mm. This results in total of 27.59L.

However, this analysis does not give the actual accurate dimensions of the DC-DC as the cooling part is missing. Further, a PCB design with a cooling strategy can be done for

more accurate results.

## 4.2 Design B

### 4.2.1 Non-isolated buck-boost converter

A design B has a fuel cell of 100kW capacity. Also, the input voltage to the DC/DC converter is a nominal voltage of 300V. The DC link voltage at the output of the DC/DC converter is maximum 378 V. The varying voltage requirements within the limits of 252-378 V makes it necessary to design a buck-boost converter.

#### 4.2.1.1 Simulation

A three phase interleaved buck boost was chosen due to the high power requirement and also low current ripples.

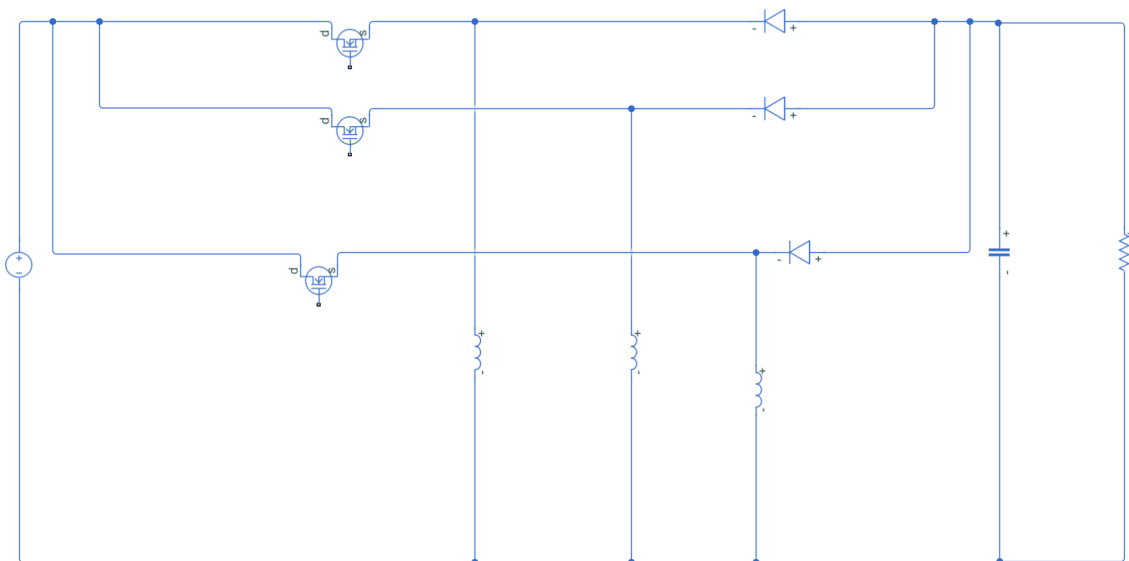


**Figure 4.36:** Three phase buck boost converter

Figure 4.36 shows a 3 phase Buck Boost converter topology used for the 100 kW fuel cell stack. The output voltage and current is always inverted according to the (2.27). A 3 phase topology was chosen for simplicity and the division of the high input current through the MOSFET's. The input voltage is 90 V and the duty cycle for the simulation is 0.6 as the expected output value of 378 V occurs at this duty cycle.

## 4. Analysis

---

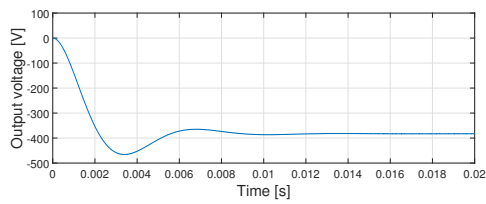


**Figure 4.37:** Output voltage- three phase buck boost converter

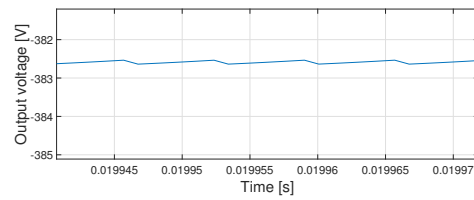


**Figure 4.38:** Ripple voltage- three phase buck boost converter

Figure 4.37 shows that the average output voltage is 382 V which is the expected value and Figure 4.38 shows the ripple value of 0.1 V peak to peak.

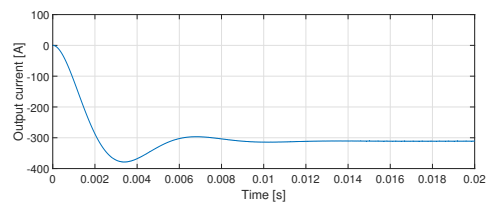


**Figure 4.39:** Output current- three phase buck boost converter

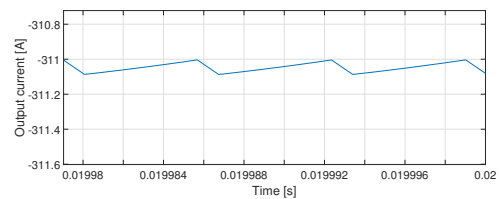


**Figure 4.40:** Ripple current- three phase buck boost converter

Figure 4.39 and Figure 4.40 show the average output current of 311 A and a ripple value of 0.08 A peak to peak respectively.

# 5

## Conclusion

The isolated and the non isolated DC/DC converters for a fuel cell vehicle with a fuel cell stack of 45kW output power and an electric battery of 9.5kWh energy have been designed and simulated.

The placement of the air compressor to supply  $O_2$  to the fuel cell stack affect the direction of the power flow of the DC/DC converter. In this thesis, it is concluded that the unidirectional topology gives a simple control, reliable function and less cost. Even though the efficiency was not analyzed, from the fact that the dual active bridge enables soft switching, the efficiency will be higher than in the unidirectional topology.

When it comes to the isolated converter topology for Design A, a unidirectional regulated DC/DC converter with the full bridge on the primary side and the full wave bridge on the secondary side was selected. On the other hand, for a non-isolated topology, a three-phase boost converter was selected to compare efficiency, cost and volume and also for the simplicity of control compared to other non-isolated topologies.

In the fuel cell vehicle system with the CX 11 platform, one fuse and one isolation relay at the fuel cell negative pole between the fuel cell stack and the DC/DC converter is installed to protect high current to the DC/DC converter primary side when having faults on a fuel cell stack. Also, in the case that a fuel cell stack should not produce electric current but it still produces due to faults on such as fuel tank valves, a discharge relay and discharge resistors are connected to a fuel cell stack in parallel.

### 5.1 Efficiency

In efficiency-wise, unisolated converters showed higher efficiency than isolated converters. The isolated converter with the selected components is maximum 95.3 % efficient in Figure 4.11. The non isolated converter with the selected components is maximum 99.0 % efficient in Figure 4.32. However it is also observed that the efficiency varies with the output voltage from the fuel cell.

### 5.2 Cost Analysis

In cost-wise, a three-phase nonisolated boost converters had a higher cost compared with all the combinations in the isolated converter whereas the cost of a four-phase nonisolated boost converter depends on the components selection in the isolated converter. However, since unisolated converters cannot protect the fuel cell stack from overvoltage coming from the battery side or the inverter side, the contactors should be placed between the fuel cell stack and the DC/DC converter. However, even with two isolation contactors between the fuel cell stack and the DC/DC converter, when the car is running, the fuel cell stack is not protected against overvoltage.

In case of a short circuit, there is a risk of blowing the whole fuel cell if all the safety components fail. Also, there is an increased complexity in the control strategy of the safety components. Thus, selecting the isolated solution gives a bit more expensive but overall a more safer solution than the unisolated one.

A Dual active bridge can be used when two way of power flow is required, for instance depending on the power source of the air compressor. When the power source of it is a battery, it consumes energy so the battery should be charged frequently. Thus, the air compressor can be connected to the fuel cell stack. However, at first, the fuel cell does not have enough power to power up the air compressor. This leads to two way of power flow where only one input to the air compressor is required. In this case for higher efficiency, case III has been used.

A Dual active bridge also provides soft switching, decreasing the switching losses. On the other hand, when there is two ways of current paths to the air compressor, there is no need of bidirectionability in the DC/DC converter which increase the risk of malfunctioning and complexity of the control.

### 5.3 Volume Analysis

Volume-wise, the unisolated DC-DC converter have a smaller volume than the isolated one. The transformers or the inductors and the capacitors occupy the largest space in converters. Two isolated converters in parallel occupy 8.9 *liters* more space than the three phase non isolated boost converter with 2D drawings with Visio. When it comes to The reason for this is that the isolated boost has almost twice the number of components as compared to the three-phase non isolated boost converter such as heat sinks, MOSFETs, diodes and so on.

Also, the switching frequency plays an important role when it comes to the volume analysis. The switching frequency in this thesis for both the isolated and non-isolated converters is fixed at 50kHz. This is because for the isolated converter, changes in the frequency does not affect much when it comes to the size of the transformers as can be seen in Figure 4.6. The volume at 10kHz is 1.68 *Liters*, 1.25 *Liters* at 50kHz, and 1.2 *Liters* at 100kHz

are observed. However, a 2 % of efficiency changes occurred when going from 20kHz to 50kHz while 4 % of efficiency changes from 50kHz to 100kHz according to Figure 4.6.

In the non-isolated converter, 50kHz is a good option since the size of the boost inductors as function of switching frequency in Figure 4.25 shows that the volume at 10kHz, at 50kHz, and at 100kHz, remain the same.



# 6

## Future work

Development of a DCDC converter especially for a new topic such as a fuel cell car requires a lot of technical analysis and limited time has put some constraints on the work. This section focuses on the advancements that can be done in the future.

**Controller.** An open loop simulation is discussed in this thesis. Further, a close loop feedback could be implemented using a PWM controller which will help in controlling the phase angle between the MOSFETs.

**Thermal analysis.** Better cooling strategies will give a clearer view of the volume occupied by the DC/DC converter.

**Improvement in component selection.** SiC and GaN material MOSFETs could be implemented for lowering the losses. Also development of a fuel cell model with more information could be done.

**Snubber circuit and soft switching.** Snubber circuit was not implemented to reduce stress on the switching device in this thesis. Also, with the improved control and safety requirement, soft switching can be implemented.

**Protection schemes.** Protection schemes such as ASIL class, graceful degradation could be analysed to see the limitations of the converter.

**Prototype.** A PCB design could be done and then tested for improved knowledge on the volume occupied by the isolated and the unisolated converter. Also the simulation results could be thus verified.

**Possible combinations for the fuel cell car.** Different matrix combinations of different battery capacity, fuel cell power and DC-DC can be used to see the performance.

**Varying voltage drive system.** Benchmarking without the converter (Varying Voltage drive system) could be a task where analysis of the whole system without the DC-DC converter can be taken into consideration.



# Bibliography

- [1] What is WLTP and how does it work?  
<http://wltpfacts.eu/what-is-wltp-how-will-it-work/>
  
- [2] Gargies, S., Wu, H. and Mi, C. (2006) 'Isolated bidirectional DC/DC converter for hybrid electric vehicle applications',  
The Sixth Intelligent Vehicle Symposium, Traverse City, MI, June 12±16.  
<https://apps.dtic.mil/dtic/tr/fulltext/u2/a521655.pdf>
  
- [3] Purvins, Arturs Krievs, Oskars Steiks, Ingars Ribickis, Leonids. (2006). Design of power circuit of DC/DC step-up converter for a PEM fuel cell. [online]  
<https://www.researchgate.net/publication/228409185>
  
- [4] Kreutzer, Otto Maerz, Martin Eckardt, Bernd. (2014). Unidirectional fast switching non-isolated 100 kW fuel cell boost converter. 10.1109/EPE.2014.6910797.  
<https://www.researchgate.net/publication/282136553>
  
- [5] Qian Xun, Yujing Liu, Elna Holmberg  
*A Comparative Study of Fuel Cell Electric Vehicle Hybridization with Battery or Supercapacitor 06/2018* 10.1109/SPEEDAM.2018.8445386
  
- [6] S.M. Haile  
*Schematic fuel cell polarization (voltage vs. Current density) and power density curves. Fuel Cell Materials and Components, Acta Materialia, Vol. 51, 2003, 5981-6000*
  
- [7] MOSFET theory  
<https://sv.wikipedia.org/wiki/MOSFET>
  
- [8] Rohm Semiconductors Calculation of power loss (Synchronous)  
[http://rohms.rohm.com/en/products/databook/applinote/ic/power/switching\\_regulator/powerlossappli](http://rohms.rohm.com/en/products/databook/applinote/ic/power/switching_regulator/powerlossappli)
  
- [9] Vacuumschmelze  
<https://www.vacuumschmelze.de/en/products/cores-components/applications/cores/nanocrystalline-cut-cores-made-of-vitroperm-500-for-power-transformers.html>

- [10] William T McLyman, Colonel. (2019).  
*Transformer and inductor design handbook* / Colonel Wm. T. McLyman. SER-BIULA (sistema Librum 2.0).
- [11] FINEMET ® F3CC Series Cut Core, Hitachi Metals  
<http://www.hitachi-metals.co.jp/e/products/elec/tel/p1308.html>
- [12] WireTronic Inc.  
<https://wiretron.com/litz-wire/>
- [13] MWS Wire Industries  
<https://mwswire.com/specialty-wire/litz-wire/>
- [14] OSCO Ltd  
<http://www.osco.uk.com/products/cable-and-litz-wire/litz-wire-winding-wire>
- [15] Copper Wire Tables (Technical report).  
*Circular of the Bureau of Standards No.31 (3d ed.). United States Department of Commerce. October 1, 1914.*
- [16] Mohan Power electronics  
<http://uni-site.ir/khuelec/wp-content/uploads/Mohan-Power-Electronics.pdf>
- [17] Kang, Yonghan. (2019).  
*Design and Implementation of High Efficiency, High Power Density Front-End Converter for High Voltage Capacitor Charger.*
- [18] N. Mohan, T. Undeland, and W. Robbins,  
*Power Electronics – Converters, Applications, and Design, 2nd ed. New York: Wiley, 1995, Ch. 7*
- [19] R. Jez,  
*"Influence of the Distributed Air Gap on the Parameters of an Industrial Inductor," in IEEE Transactions on Magnetics, vol. 53, no. 11, pp. 1-5, Nov. 2017, Art no. 8401605. doi: 10.1109/TMAG.2017.2699120*  
URL: <http://ieeexplore.ieee.org/stamp/stamp.jsp?tp=arnumber=8082157isnumber=8082142>
- [20] PCB CREEPAGE CALCULATOR  
<https://pcbdesign.smps.us/creepage.html>
- [21] Heat sink  
<https://www.cui.com/blog/how-to-select-a-heat-sink>
- [22] Heat sink calculations  
<http://www.giangrandi.ch/electronics/thcalc/thcalc.shtml>

[23] Fuel cell vehicles

*[https://en.wikipedia.org/wiki/Fuel\\_cell](https://en.wikipedia.org/wiki/Fuel_cell)*

[24] RoHS directives

*<https://www.rohsguide.com/>*

[25] Facts about Lithium ion batteries

*<http://gridedge.com.au/assets/facts-about-lithium-ion-batteries-20151108.pdf>*

